NBS-GCR-79-188

AN INVESTIGATION OF FIRE IMPINGEMENT ON A HORIZONTAL CEILING

H.Z. You and G.M. Faeth

OCTOBER 1978

Issued DECEMBER 1979

Sponsored by
U.S. Department of Commerce
National Bureau of Standards
Washington, DC 20234

NBS-GCR-79-188

AN INVESTIGATION OF FIRE IMPINGEMENT ON A HORIZONTAL CEILING

H.Z. You and G.M. Faeth

Mechanical Engineering Department
Pennsylvania State University
University Park, Pennsylvania

October 1978

Issued December 1979

Grant Number 7-9020

Sponsored by

Center for Fire Research
National Bureau of Standards
Washington, DC 20234

Notice

This report was prepared for the Center for Fire Research of the National Engineering Laboratory, National Bureau of Standards under Grant No. 7-9020. The statements and conclusions contained in this report are those of the authors and do not necessarily reflect the views of the National Bureau of Standards or the Center for Fire Research.

An Investigation of Fire Impingement on a Horizontal Ceiling

by

H.Z. You and G.M. Faeth

Mechanical Engineering Department
The Pennsylvania State University
University Park, Pennsylvania

Prepared for

U.S. Department of Commerce

National Bureau of Standards

Center for Fire Research

Grant No. 7-9020

Dr. Howard Baum, NBS Scientific Officer

October, 1978

An Investigation of Fire Impingement on a Horizontal Ceiling

Summary

This report discusses research completed under NBS Grant No. 7-9020, during the period September 1, 1977 to August 31, 1978. The investigation considers the processes which occur when a turbulent fire impinges upon a horizontal ceiling. Measurements were conducted to determine free flame heights, impinging flame lengths along the ceiling, ceiling heat fluxes and mean temperature distributions in the flow. Both unconfined and confined ceilings were considered. Theoretical analysis was completed in order to suggest simple methods for correlating the data.

The fire source was simulated by burning wicks soaked with liquid fuel (methanol, ethanol, 1-propanol and n-pentane). The range of test variables involved ceiling diameters of 610-660 mm, ceiling heights of 58-940 mm, wick diameters of 10-107 mm and curtain wall heights (for confined ceilings) as large as the ceiling height.

The results of the various aspects of the study can be summarized as follows:

1. Free Flame Heights. Free flame heights were studied since it was found that radial flame spread for a flame impinging on a ceiling was related to the free flame height. The present free flame heights could be correlated by the following expression:

$$H_f/D = 10.96\ N_{CO}^{0.211} \qquad \text{(I)}$$

This equation is based on the combusting plume analysis of Steward (29). The present values of free flame height are somewhat lower than other values in the literature due to the reduced luminosity of alcohol flames and different source characteristics.

2. Impinging Flame Lengths. The radial distance that an impinging flame extends along a ceiling could be correlated as follows for an unconfined ceiling:

$$H_R/D = 0.502[(H_f-H)/D]^{0.957} \qquad \text{(II)}$$

where H_f/D is found from Eq. (I). The total length of an impinging flame, $H+H_R$, is somewhat less than the free flame height.

The radial spread is larger when the ceiling is confined, due to the reduced oxygen concentration within the ceiling layer. In this case the radial spread is:

$$H_R/D = 0.692[(H_f-H)/D]^{0.887} \qquad \text{(III)}$$

3. Ceiling Heat Flux. The heat flux to the ceiling from a turbulent impinging plume or fire was relatively constant in the stagnation region, $r/H<.2$. For values of $H_f/H<1.5(H_R/H<.25)$, the following correlation was obtained for unconfined ceilings.

$$\dot{q}''H^2/\dot{Q} = 31.21\ Pr^{-3/5}Ra^{-1/6} \qquad \text{(IV)}$$

For larger values of H_f/H, the heat flux declines from the value given by Eq. (IV), since the cooler core region of the fire impinges at the stagnation point.

Equation (IV) is based on an analysis by Donaldson, et al (30) for the heat transfer rate of a turbulent impinging jet. Comparing

the heat fluxes for the same value of maximum velocity, temperature difference and radial width of the flow (prior to impingement) indicates that the heat flux from a jet is 2.6 - 4.2 times larger than that of the plume. In many respects, the flows are similar, e.g., the turbulent intensities are about the same. The major factor in this behavior could involve flow stratification near the stagnation point for the buoyant flow; however, further study will be required to resolve this behavior.

A theoretical estimation of the stagnation point heat flux for laminar flow was also obtained, as follows:

$$\dot{q}''H^2/\dot{Q} = 0.0136\ Pr^{-3/5}Ra^{3/8} \qquad \text{(V)}$$

Only turbulent flow was examined during the present tests. $Ra > 10^9$ and Eq. (V) could not be verified experimentally. The predictions of Eq. (V) yield much higher stagnation point heat fluxes for laminar flow than for turbulent flow, due to reduced mixing rates in laminar plumes. The heat flux also increases with increasing Rayleigh number for laminar flow, in contrast to turbulent flow, Eq. (IV) where the opposite trend is observed.

For $r/H > .2$, Alpert's theoretical model, employing a constant friction factor of 0.03, agreed with the data for unconfined ceilings. The measurements can also be correlated by the following expression:

$$\dot{q}''H^2/\dot{Q} = 0.04(r/H)^{-1.3} \qquad \text{(VI)}$$

This correlation was equally successful for impinging flames, in the range $H_R/H < .06$.

The heat fluxes are increased when the ceiling is confined; however, Eqs. (IV) and (VI) still provide a reasonable estimation of heat flux values. Work currently in progress is considering the extension of the models to the confined ceiling flow, in order to improve the accuracy of the correlations under these conditions.

4. Mean Temperature Distributions. Mean temperature distributions were measured in the plume, the ceiling jet and the ceiling layer (if present) for both unconfined and confined ceilings. The value of $H_f/H = .14$ was used for these tests, so that the bulk of the measurements are in the weakly buoyant region of the flow.

Temperature levels and widths of the plume compared favorably with existing correlations reported by Rouse, et al (32), George, et al (38) and Yokoi (34), although the present measurements agreed best with Ref. 32. For the unconfined ceiling, temperature levels in the ceiling jet were predicted within 20% using Alpert's (23, 24) model (assuming a friction factor of 0.03, found from heat flux measurements. The model tends to underestimate the width of the flow, however.

Work is in progress to extend Alpert's (23, 24) model to the case where a ceiling layer is present. Current theories were capable of estimating the temperature level within the stratified layer within 15-30%, depending on whether the plume correlation of Refs. 32, 24 or 38 was used. The correlation of Ref. 38 was best in this case, although heat losses during the present tests might have caused fortuitously good agreement.

The conclusion of this initial phase of the investigation of fire

impingement on ceilings has provided some useful, simplified correlations for important parameters in the flow, represented by Eqs. (I)-(VI). Current work is considering a more rational treatment of the effect of the ceiling layer and the influence of flow structure of the heat transfer characteristics of impinging fires.

Acknowledgement

This research was supported by the United States Department of Commerce, National Bureau of Standards, Grant No. 7-9020. Dr. Howard Baum of the Center for Fire Research was the NBS Scientific Officer for the project.

Table of Contents

	Page
Summary	i
Acknowledgement	vi
List of Tables	viii
List of Figures	ix
Nomenclature	x
1. Introduction	1
1.1 Fire Models	1
1.2 Previous Studies of Plume Impingement	3
1.3 Objectives of the Study	4
2. Experimental Apparatus and Procedure	4
2.1 Ceiling Heat Flux Measurements	5
2.1.1 Test Arrangement	5
2.1.2 Instrumentation	5
2.1.3 Procedure	9
2.2 Flame Length Measurements	9
2.3 Temperature Distribution Measurements	10
2.3.1 Test Arrangement	10
2.3.2 Instrumentation	11
2.3.3 Procedure	11
3. Theory	13
3.1 Free Flame Height Correlation	13
3.2 Ceiling Heat Flux Correlation	14
3.2.1 Correlation for Stagnation Region	14
3.2.2 Correlation for r/H>0.2	17
4. Results and Discussion	20
4.1 Flow Visualization	22
4.2 Flame Height	25
4.3 Flame Length Along Ceiling	25
4.4 Ceiling Heat Flux	28
4.5 Mean Temperature Distributions	40
References	51
Appendix Tabulation of Data	55

List of Tables

Table	Title	Page
1	Parameter Values for Ceiling Jet	20
2	Physical Properties of Fuels	21
3	Comparison of Turbulent Impinging Jets and Plumes at the Stagnation Point	32
4	Plume Profile Constants	44
5	Summary of Plume Characteristics	45
6	Summary of Ceiling Jet Characteristics	47
7	Predicted and Measured Ceiling Layer Temperatures	50
A-1	Free Flame Height Data	56
A-2	Flame Length Along Ceiling (No Curtain Wall)	58
A-3	Flame Length Along Ceiling (Curtain Wall)	60
A-4	Stagnation Point Heat Transfer Rates for Plume Impingement on an Unconfined Ceiling	62
A-5	Effect of Flame Impingement on Stagnation Point Heat Transfer Rates on an Unconfined Ceiling	64
A-6	Ceiling Heat Fluxes for Plume Impingement on an Unconfined Ceiling	66
A-7	Ceiling Heat Fluxes for Flame Impingement on an Unconfined Ceiling	70
A-8	Ceiling Heat Fluxes for Plume Impingement on a Confined Ceiling (L = 152 mm)	75
A-9	Ceiling Heat Fluxes for Plume Impingement on a Confined Ceiling (L = 305 mm)	78
A-10	Ceiling Plume Temperatures (No Curtain Wall)	80
A-11	Ceiling Jet Temperatures (No Curtain Wall)	83
A-12	Ceiling Plume Temperatures (Curtain Wall, L = 241 mm, D_c = 610 mm)	88
A-13	Ceiling Jet Temperatures (Curtain Wall, L = 241 mm, D_c = 610 mm)	91

List of Figures

Figure	Caption	Page
1	Sketch of the Experimental Apparatus for Heat Transfer Measurements	6
2	Sketch of the Wall Heat Flux Transducer	8
3	Sketch of the Temperature Probe	12
4	Photograph of an n-pentane Fire Impinging on an Unconfined Ceiling. H = 214 mm, D = 91 mm (square), $\dot{Q}$ = 7.54 kW	23
5	Shadowgraph of a Turbulent Propanal Fire Plume Impinging on an Unconfined Ceiling. H = 165 mm, D = 18 mm, $\dot{Q}$ = 0.2 kW	24
6	Shadowgraph of a Laminar Propanol Fire Impinging on an Unconfined Ceiling. H = 75 mm, D = 51 mm, $\dot{Q}$ = 0.8 kW	26
7	Free Flame Heights	27
8	Flame Lengths along a Ceiling	29
9	Stagnation Point Heat Transfer Rates for Plume Impingement on an Unconfined Ceiling	30
10	Effect of Flame Impingement on Stagnation Point Heat Transfer Rates on an Unconfined Ceiling	35
11	Ceiling Heat Fluxes for Plume Impingement on an Unconfined Ceiling	37
12	Ceiling Heat Fluxes for Flame Impingement on an Unconfined Ceiling	38
13	Ceiling Heat Fluxes for Plume Impingement on a Confined Ceiling	39
14	Temperature Distributions in the Plume and the Ceiling Jet for an Unconfined Ceiling	41
15	Temperature Distributions in the Plume and the Ceiling Jet for a Confined Ceiling	42

Nomenclature

Symbol	Description
C_p	specific heat
C_T	plume parameter, Eq. (48)
C_w	plume parameter, Eq. (47)
D	wick diameter
D_c	ceiling diameter
E	ceiling jet entrainment constant
E_p	plume entrainment constant
f	friction factor
g	gravitational acceleration
h	ceiling jet characteristic width, Eqs. (18)-(20)
$\bar{h}_e$	parameter, Eq. (27)
H	ceiling height
H_f	free flame height
H_R	radial extent of flame under ceiling
K	parameter, Eq. (28)
K_f	parameter, Eq. (2)
ℓ, ℓ_T	characteristic ceiling jet radius, Eqs. (31)-(33)
ℓ_p, ℓ_{pT}	characteristic plume radius, Eq. (30)
L	length of curtain wall
$\dot{m}$	plume mass flow rate
$\dot{m}_F$	fuel mass flow rate
N_{CO}	parameter, Eq. (3)
P_r	Prandtl number
$\dot{q}''$	heat flux

Symbol	Description
$\dot{Q}$	plume thermal energy flux
Q_c	heat of combustion
r	radial distance
$\bar{r}$	normalized radial distance, r/H
$\bar{r}_e$	parameter, Eq. (26)
r_s	stoichiometry parameter, mass of air to mass of fuel
$r_{1/2}$	plume half width
Ra	Rayleigh number, Eq. (11)
Ri_e	Richardson number, Eq. (25)
T	temperature
v	radial velocity parallel to ceiling
V	characteristic velocity Eqs. (18)-(20)
w	vertical velocity
y	distance from ceiling
z	height above source
α	parameter, Eq. (6)
β	coefficient of thermal expansion
β'	parameter, Eq. (30)
γ	parameter, Eq. (32)
∇	characteristic temperature defect, Eqs. (18)-(20)
μ	viscosity
ν	kinematic viscosity
ρ	density
ϕ	parameter, Eq. (24)
ω	parameter, Eq. (4)

Subscripts	Description
c	centerline of plume
e	edge of boundary layer
lam	laminar
max	maximum
o	value at fuel source
p	plume
w	wall
∞	ambient

1. Introduction

1.1 Fire Models

The widespread use of computers has provided greater acceptance of models which simulate extremely complex processes as tools for design and interpretation. This has also been the case for problems of fire prevention and control, leading to the development of models which attempt to predict the history of fires within structures. The models assist our understanding of fire dynamics, but also have the practical objective of providing a means of evaluating fire hazards, detection methods, the impact of new materials on potential fire hazards, etc., without resorting to expensive large-scale testing. Recent reports of comprehensive fire models include Emmons and coworkers (1)*, Zukoski and Kubota (2), Smith and Clark (3), Lloyd and coworkers (4) and Tanaka (5). Similar modeling efforts are in progress elsewhere.

Comprehensive fire models are constructed by combining more specific models of subprocesses within the fire environment. Typical subprocesses include: material burning rate models, fire plumes, radiation and convection within the structure, etc. Earlier work completed in this laboratory has considered the subprocesses involving the rate of burning of upright surfaces, heat transfer rates between the fire plume and the unburned surface above the actively burning area, and the structure of a fire plume along an upright surface (6-16). The experimental results were successfully correlated with relatively simple analytical models which can be used within more comprehensive models of the fire environment.

---

*Numbers in parenthesis denote references.

Another important subprocess in the fire environment involves impingement of a fire plume on a ceiling. This process occurs during most unwanted fires within structures. An object within the structure is ignited and a fire begins to grow. As the fire plume rises from the source, the first structural element that it contacts is the ceiling. In the early stages, the flames are relatively short and only heated plume gases reach the ceiling. As fire growth continues, however, the flames eventually reach the ceiling and are deflected along its surface. Impingement of the flames on the ceiling greatly modifies the flame shape and the heat transfer characteristics within the enclosure. Clearly, the occurrence of flame impingement is an important signal event in the history of a fire.

Ceilings are usually confined by walls at their extremities. In this case, hot gases, combustion products, etc., accumulate in a stratified ceiling layer. The depth of this layer is controlled by the strength of the fire, and the availability of openings, doors, windows, etc., through which the hot gases can be vented. A fire plume passing the lower edge of the ceiling layer, finds itself in a new ambient environment. Therefore, the presence of a stratified ceiling layer can significantly modify the characteristics of the plume, and in this manner influence heat transfer rates, etc., in the vicinity of the ceiling.

The present investigation is a contribution to the problem of fire impingement on a ceiling. In the following, previous studies of this process are reviewed, prior to a description of the specific objectives of the present investigation.

1.2 Previous Studies of Plume Impingement

Several investigations of confined plumes from relatively small buoyant sources have been reported (4, 17-20), although these studies have not dealt with heat transfer characteristics in any detail. Numerous studies of heat transfer from jets impinging on plane surfaces have been reported; however, the absence of buoyancy and flow stratification limits the relevance of this work to the fire plume impingement problem.

A few studies have considered relatively unconfined plume impingement on a ceiling. Thomas (21) and Pickard, et al (22) completed limited measurements of temperatures and velocities within impinging plumes; however, one of the most comprehensive studies of impinging plumes is the work of Alpert (23, 24) at Factory Mutual Research Corporation. Alpert considered both axisymmetric and line fire sources, although experiments were limited to axisymmetric flows. An integral model was developed for the process. Predicted plume temperature and velocities compared favorably with measurements in both model size (.3 - 1 m ceiling height) and full size (2.4 - 15.9 m ceiling height) experimental arrangements. Only limited heat transfer measurements were made in this study, under conditions that could not be controlled to a great degree; however, these results do show an encouraging degree of agreement with the theory.

Zukoski, et al (25) investigated the characteristics of both unconfined and confined plumes. The distribution of heat flux to the ceiling and the temperature distribution in the ceiling jet were considered. The results for unconfined plumes tend to confirm Alpert's (23, 24) earlier

findings for the region beyond the turning point. However, only limited information was generated concerning the effect of the ceiling layer formed under confined ceilings and fire impingement was not treated.

1.3 Objectives of the Study

The review of earlier studies indicates that a number of investigators have measured ceiling heat fluxes resulting from plume impingement. Correlations are available for predicting these heat fluxes for unconfined ceilings in the region beyond the turning point. Results for the stagnation region, the effect of ceiling layers, and fire impingement on a ceiling has not received much attention in earlier work.

With this status in mind, the objectives of the present investigation were as follows:

1. Determine flame heights for impinging plumes and the radial extent of the flame under the ceiling for impinging fires.
2. Measure ceiling heat fluxes for impinging plumes and fires.
3. Measure mean temperature distributions within both the plume and the ceiling jet.

Both confined and unconfined ceilings are considered. While the investigation emphasizes the accumulation of experimental results, analysis was undertaken to the extent required to obtain convenient methods of data correlation.

2. Experimental Apparatus and Procedure

Two different arrangements were used for the experiments: (1) a transient apparatus for measuring wall heat fluxes, flame heights, and flame lengths along the ceiling, and (2) a steadily operating apparatus

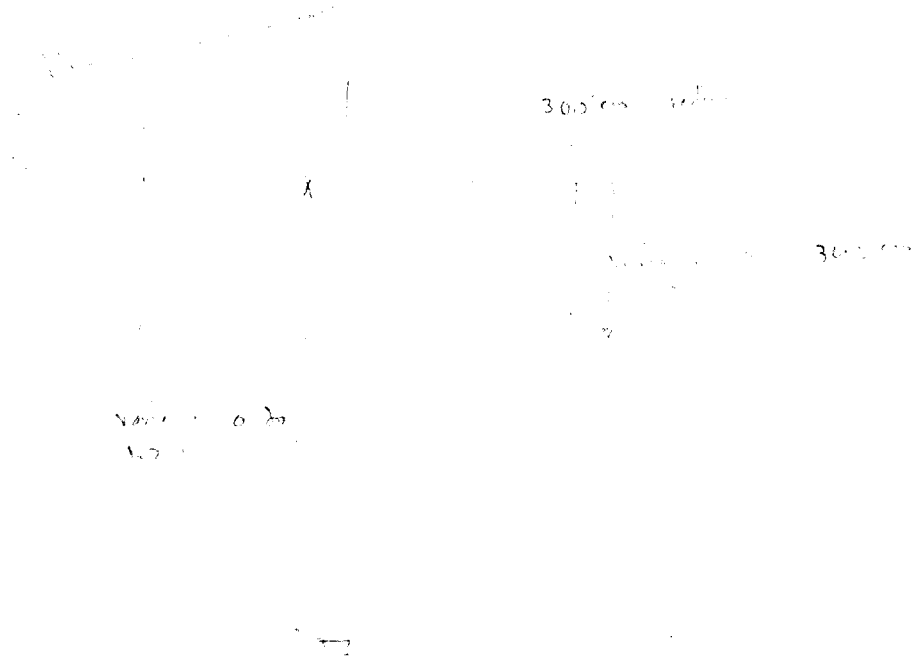

for measurements of the mean temperature profiles within the flow.

2.1 Ceiling Heat Flux Measurements

2.1.1 Test Arrangement

The apparatus is illustrated schematically in Figure 1. The fire source is provided by burning methanol, ethanol, 1-propanol, or n-pentane on the top surface of cylindrical wicks of various diameters. The wicks were constructed from an insulating material, Fiberfrax Hot Board, Carborundum Company, similar to earlier work with wall fires (16). The periphery of the wicks was carefully wrapped with aluminum foil and electrical tape so that the flame was confined to the upper surface.

The ceiling was constructed of a copper plate, 660 x 660 mm, 9.5 mm thick. The total heat flux, convective and radiative, was measured. Therefore, the front surface of the ceiling was coated with a radiation absorbing paint (3 M Nextel 101 C-10) having an emissivity of 0.96. The rear surface of the ceiling was insulated with a 50 mm thick layer of Fiberfrax Lo-Con blanket, coated with aluminum foil.

A curtain wall having a diameter of 610 mm was used to examine the effect of confinement. The wall was constructed of 0.8 mm thick aluminum sheet. The distance between the lower edge of the curtain wall and the ceiling could be adjusted in the range 0-305 mm.

The ceiling was supported from a movable frame which allowed ceiling heights to be varied in the range 0-1200 mm.

2.1.2 Instrumentation

The burning rate of the fuel was determined by continuously measuring the weight of the fuel-soaked wick with a load cell (UniMeasure/80 multi-purpose transducer). The load cell was powered by a 6-V battery and combined with a circuit allowing sensitivity adjustment and zero suppression.

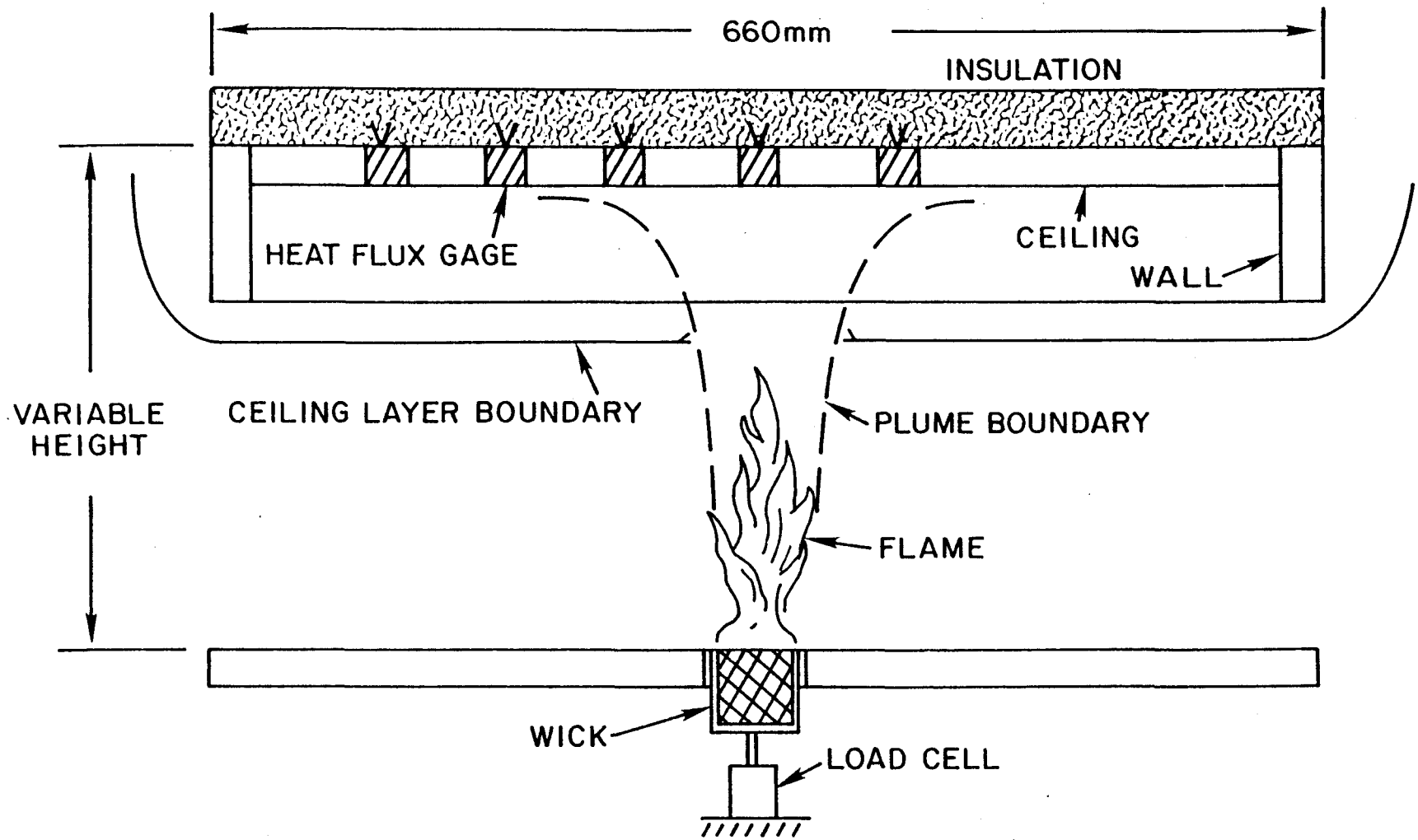

Fig. 1 Sketch of the Experimental Apparatus for Heat Transfer Measurements.

The dc voltage output was read through a multimeter (Model 1240, Weston Instrumentation, Inc.). Before taking any measurements, the load cell was carefully calibrated with standard weights in the measured range.

The burning rate of the fuel was found to be constant for most of the test conditions. Therefore, measuring the initial and final weight of the wick and the time of burning provided a simple determination of the burning rate of the fuel.

The total heat flux to the ceiling was measured by sensors which were located at several radial positions. A sketch of a typical sensor is shown in Figure 2. The sensors were cylindrical copper plugs, painted with the high emissivity point on the front surface. By measuring the rate of temperature rise of these plugs after ignition of the flame, the heat fluxes could be calculated from the known thermal capacity of the plugs. Since the Biot number of plugs is very small for the present test conditions, the temperature is essentially uniform in each plug at each instant of time.

The temperatures of the plugs were measured with chromel-alumel thermocouples (26 gage, Omega Engineering, Inc.) which were attached to their rear surface. The thermocouple leads were passed horizontally along the ceiling, under the insulation, in order to reduce errors due to conduction and convection. In order to reduce the lateral heat transfer between the ceiling and the plugs, the periphery of the plugs was insulated from the ceiling with Fiberfrax Lo-Con Blanket. The radial conduction error of the sensors was monitored by measuring the temperature of the ceiling adjacent to the plugs. Corrections were then made to account

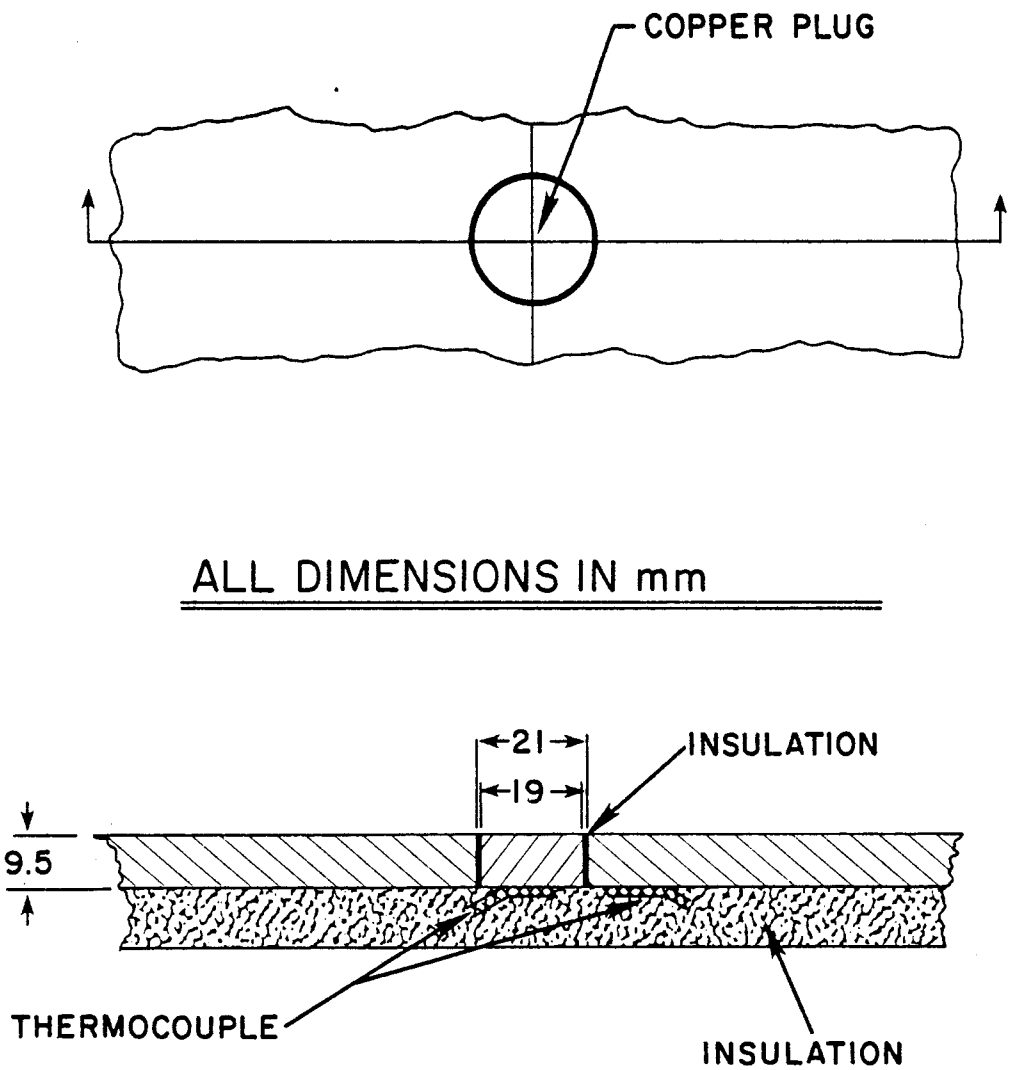

Fig. 2 Sketch of the Wall Heat Flux Transducer.

for radial heat transfer across the insulated gap.

The output of the load cell was read with a digital multimeter, and the outputs of the thermocouples were recorded with a CEC, Type 5-124 Recording Oscillograph.

2.1.3 Procedure

Since a buoyant fire plume is very sensitive to outside disturbances, all the experiments were done in a draft-free room. In order to reduce the disturbances to a minimum, all instrumentation and the test operator were located as far from the fire source as possible. The test frame was also surrounded with a layer of fine wire net (16 mesh) to reduce ambient disturbances.

After the wick was saturated with fuel, it was ignited. As soon as the flame became steady, the initial total weight of the wick was recorded and the instantaneous temperatures of the plugs were measured for a period of time. At the end of each measurement the final total weight of the wick was recorded, to provide the burning rate of fuel. After the wall had cooled, this process was repeated for the next test. The data reported at each location is the average of three tests.

2.2 Flame Length Measurements

Three flame lengths were measured: (1) the free flame length with no ceiling present, (2) the length of non-impinging flames with the ceiling present, and (3) the radial distance that an impinging flame extends along the underside of a ceiling. These tests were conducted in a darkened room, using the apparatus employed for the heat flux measurements. In all cases, flame lengths and the burning rate of the wick were measured simultaneously.

Free flame lengths and the length of non-impinging flames were measured with a straight rule, fixed at some distance from the flame. The lower end of the rule was mounted flush with the surface of the wick. There were two markers on the rule which could slide up and down freely. The flame was observed for a period of time and the positions of the markers were adjusted to indicate the highest and lowest positions of the flame tip. The flame height was taken to be the arithmetic average of these two limits. Each flame height that is reported is the average of two independent measurements.

The radial length along the ceiling of impinging flames was measured by mounting two fine wires perpendicular to each other and passing through the geometrical center of the ceiling. There were four markers on each wire, two on each side of the centerline. The markers were located at the maximum and minimum flame tip position in each direction. The average value of the distances in both directions is the reported flame length. Each radial length that is reported is the average of two independent measurements.

2.3 Temperature Distribution Measurements

2.3.1 Test Arrangement

These measurements employed the same apparatus as the heat flux measurements, except that the wick was fed continuously with fuel. The apparatus was not cooled; therefore, the measurements are more representative of an adiabatic ceiling. Relatively low flame heights were employed for these tests in order to minimize the temperature levels of the ceiling, and thus radiative heat losses from the surface.

The fire source was constructed of a 20 mm I.D. stainless steel tube packed with wicking (Fiberfrax Hot Board, Carborundum Company).

The outer surface of the tube was insulated. The bottom of the tube was continuously supplied with fuel from a constant head storage container.

2.3.2 Instrumentation

The thermocouple probe illustrated in Fig. 3 was used to measure mean gas temperatures. A chromel-alumel junction was employed, constructed of 25.4 μm diameter wires. The fine wires were first attached to 0.81 mm diameter lead wires by spark welding. The junction was then formed by welding the fine wires with a microtorch. For the present range of test conditions, this junction has a negligible radiation correction.

The thermocouple output was recorded with a Hewlett-Packard, Model DY 2401 B Integrating Digital Voltmeter. The position of the probe was precisely adjusted by an Uni-Slide (Model A2512 CE, Velmex, Inc.).

2.3.3 Procedure

In order to measure the temperature distributions with a single probe, the measurements must be undertaken under steady state conditions. These conditions could be detected by monitoring the ceiling temperatures at several locations. When the ceiling temperatures were constant, then the desired conditions were obtained. For the present experiments ($\dot{Q}$ = 250 W, H = 695 mm), it took at least four hours to reach the steady state condition.

At each position, the mean temperature was obtained by integrating the signals over one-minute intervals. The data presented are the average of at least three measurements.

ALL DIMENSIONS IN mm

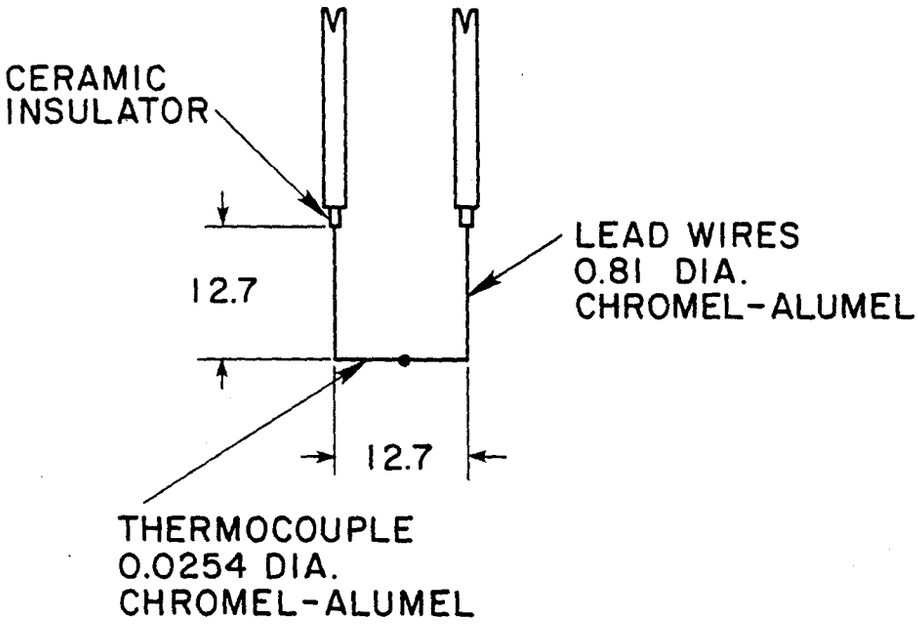

Fig. 3 Sketch of the Temperature Probe

3. Theory

Theoretical considerations involved several processes in the flow, as follows:

i. Estimation of free flame heights and the application of this information to correlate the radial extent of an impinging flame along the ceiling.

ii. Correlation of heat fluxes in the stagnation region of an impinging plume considering both laminar and turbulent plumes.

iii. Correlation of heat fluxes beyond the turning region of an impinging plume, using Alpert's approach (23, 24).

Each of these topics will be considered in this section.

3.1 Free Flame Height Correlation

The height of free turbulent buoyant diffusion flames has been studied by Thomas, et al (26), Putnam and Speich (27), Kosdon, et al (28), and Steward (29), among others. Thomas, et al (26) employed dimensional analysis to obtain parameters for correlating their experimental data. The correlation does not include fuel properties; however, for each fuel it has the following form:

$$H_f/D = f(\dot{Q}^2/D^5) \tag{1}$$

where H_f is the flame height, D is the fire source diameter and $\dot{Q}$ is the rate of heat release by the flame. Putnam and Speich (27) obtain a similar correlating expression.

Steward (29) undertook a more complete analysis of the process. An integral model was constructed assuming that the rate of combustion of the fuel was controlled by the rate of entrainment of air by the plume. This analysis yields the following expression for flame height:

$$H_f/D = K_f N_{CO}^{1/5} \tag{2}$$

where

$$N_{CO} = \frac{\dot{Q}^2 (r_s + \omega\rho_\infty/\rho_o)^2}{\rho_\infty^2 Q_c^2 g D^5 (1 - \omega)^5} \tag{3}$$

$$\omega = [1 + Q_C/ r_s C_p T_\infty]^{-1} \tag{4}$$

The remaining symbols are identified in the nomenclature. The values of the various parameters in these expressions do not vary greatly for different fuels, and Eq. (5) roughly corresponds to the result of Thomas, et al (26), given by Eq. (1).

In the following, Eq. (2) will be used to correlate free flame heights, since the relationship allows for fuel properties. The present experimental results suggest that the radial spread of impinging flames is related in a simple manner to the ratio of the free flame height to the ceiling height, H_f/H. This relationship will be examined later.

3.2 Ceiling Heat Flux Correlation

3.2.1 Correlation for Stagnation Region

In spite of its importance for modeling heat transfer in fires, earlier models of stagnation point heat transfer rates for plume impingement could not be found in the literature. More extensive results exist for impinging jets. However, these studies generally involve a heated plate exposed to a jet having a temperature equal to the ambient temperature. Therefore, the results are not directly applicable to the impingement of a heated plume on the ceiling.

The general structure of the flow near the stagnation point involves a laminar boundary layer adjacent to the wall. For a turbulent impinging flow, the ambient turbulence levels enhance the transport capabilities

of the boundary layer (30). This enhancement must be determined empirically.

Following Sibulkin (31), we obtain the following expression for the heat flux at the stagnation point of a plane body,

$$\dot{q}''_{lam} = 0.763\ Pr^{-3/5}[\rho\mu(\frac{dv_e}{dr})_{r=0}]^{1/2}\ C_p(T_e - T_w) \tag{5}$$

where v_e and T_e are the velocity and temperature at the edge of the wall layer, T_w is the wall temperature, and the usual notation is followed for physical properties.

Donaldson, et al (30) have measured the velocity gradient term required in Eq. (5) for fully developed jets. They find:

$$(\frac{dv_e}{dr})_{r=0} = \alpha\omega_c/r_{1/2} \tag{6}$$

where ω_c is the jet centerline velocity, $r_{1/2}$ is the point where the impinging jet velocity is one-half its maximum value, and $\alpha = 1.13$ for fully developed jets. In the following, we assume that Eq. (6) can be applied to plumes as well, although the value of α may be different.

Equation (5) is valid for an ambient potential flow. For impinging turbulent jets, measured heat fluxes are higher due to the influence of the ambient turbulence on the wall layer (30). The enhancement varies with the turbulence intensity, which in turn depends on the ceiling height to source diameter ratio. Therefore, we can expect:

$$\dot{q}''/\dot{q}''_{lam} = F(H/D) \tag{7}$$

Substituting Eqs. (6) and (7) into Eq. (5) yields the following expression for the stagnation point heat flux:

$$p = \frac{RT}{v} - \frac{b}{v} \quad \text{or} \quad p = \rho RT$$

$$v = \frac{RT}{p}$$

$$\Theta = \frac{1}{T} \frac{\partial}{\partial} \quad \frac{p}{R} \frac{\partial}{p}$$

$$\left(\rho \frac{\partial}{\partial} \right)^{1/2} \left(\rho c_p \Delta T \, H \nu \right)$$

$$\left[\rho \frac{\partial}{\partial} \right]$$

$$\dot{q}'' = 0.763\ Pr^{-3/5}[\rho\mu\alpha\omega_c/r_{1/2}]^{1/2}\ C_p(T_e-T_w)F(H/D) \tag{8}$$

The remainder of the analysis depends upon whether the impinging plume is turbulent or laminar. Both cases are considered in the following.

Turbulent Impinging Plume. The centerline quantities of the plume are determined at the ceiling height, neglecting virtual source effects. Rouse, et al (32) find the following relationships for axisymmetric turbulent plumes:

$$w_C H/\nu = 4.7\ Ra^{1/3} \tag{9}$$

$$g\beta(T_c - T_\infty)H^3/\nu^2 = 11.0\ Ra^{2/3} \tag{10}$$

where

$$Ra = g\beta\dot{Q}H^2/\rho C_p\nu^3 \tag{11}$$

$\beta \frac{\Delta T}{T}\ \dot{Q}H^2/\rho C_p\nu^3$

Rouse, et al (32) also find that

$$r_{1/2}/H = 0.085 \tag{12}$$

Substituting Eqs. (9)-(12) into Eq. (8) and assuming $(T_c-T_\infty) >> (T_w - T_\infty)$, yields the following expression for the heat flux at the stagnation point for a turbulent plume:

$$\dot{q}''H^2/\dot{Q} = 62.41\ \alpha^{1/2}\ Pr^{-3/5}\ Ra^{-1/6}\ F(H/D) \tag{13}$$

Equation (13) indicates that the heat flux parameter depends upon Ra, although the dependence is relatively small.

Laminar Impinging Plume. Yih (33) has presented analytical solutions for laminar plumes. For an axisymmetric plume with a Prandtl number of unity, the following equations are obtained:

$$\omega_c H/\nu = (2\pi)^{-1/2}\ Ra^{1/2} \tag{14}$$

to be the same.

Following Ellison and Turner (17), spatial averages of ceiling jet velocity, ν, and density defect, $(\rho_\infty - \rho)$, and a characteristic ceiling jet thickness, h, were defined as follows:

$$Vh = \int_0^\infty v\, dy \tag{18}$$

$$V^2 h = \int_0^\infty v^2 dy \tag{19}$$

$$V\nabla h = \int_0^\infty gv(\rho_\infty - \rho)/\rho_\infty dy \tag{20}$$

Proceeding with the above assumptions, the solution of the integral equations yields

$$V(\rho C_p H/\beta g\dot{Q})^{1/3} = (2\pi\bar{r}_e Ri_e)^{-1/3}\phi^{-(f+2E)/(f+4E)} \tag{21}$$

$$\nabla H^{5/3}(\rho C_p/\beta g\dot{Q})^{2/3} = [Ri_e/(2\pi\bar{r}_e)^2\bar{h}e^3]^{1/3}\phi^{-(Kf+2E)/(f+4E)} \tag{22}$$

$$h/H = \bar{r}_e\bar{h}_e\ \phi/\bar{r} \tag{23}$$

where

$$\phi = 1 + (f+4E)(\bar{r}^2 - \bar{r}_e{}^2)/4\bar{r}_e\bar{h}_e \tag{24}$$

$$Ri_e = 4E_p/5\sqrt{3}(\beta'^2 + 1) \tag{25}$$

$$\bar{r}_e = \frac{6}{5}\sqrt{\frac{3}{2}}\,E_p/(1 + \frac{\sqrt{3}}{5}E_p) \tag{26}$$

$$\bar{h}_e = \frac{\sqrt{3}}{5}E_p/(1 + \frac{\sqrt{3}}{5}E_p) \tag{27}$$

$$K = Pr^{-2/3} \tag{28}$$

$$\bar{r} = r/H, \quad \bar{h} = h/H \tag{29}$$

In these equations, E and E_p are the entrainment constants of the ceiling jet and the plume, respectively. The parameter β' is the ratio of the characteristic widths of the velocity and density defect profiles (the e^{-1} positions) in the plume.

$$\ell_{T_p} = \beta' \ell_p \tag{30}$$

If it is assumed that the ceiling jet velocity and temperature profiles are Gaussian, neglecting the small region involving the boundary layer at the ceiling (9),

$$\begin{aligned} v &= v_{max} \exp\left(-(y/\ell)^2\right) \\ \Delta T &= \Delta T_{max} \exp\left(-(y/\gamma\ell)^2\right) \end{aligned} \tag{31}$$

where γ measures relative widths of the two profiles in the ceiling jet (similar to Eq. (30) for the plume).

$$\ell_T = \gamma \ell \tag{32}$$

Introducing Eqs. (31) and (32) into Eqs. (18)-(20), the following relations are obtained:

$$v_{max} = \sqrt{2}\ V \tag{33}$$

$$\Delta T_{max} = (\gamma^2 + 1)^{1/2}\ \nabla / g\beta\gamma \tag{34}$$

$$\ell = \ell_T/\gamma = \sqrt{2/\pi}\ h \tag{35}$$

Employing the Reynolds/Colburn analogy, along with the preceding results, yields the following expression for the ceiling heat flux

$$\dot{q}''H^2/\dot{Q} = \frac{25 f Pr^{-2/3}}{36\pi\sqrt{2}} \left(\frac{1+\sqrt{3}\ E_p/5}{E_p}\right)^2 \phi^{-\left[\frac{(K+1)f + 4E}{f + 4E}\right]} \tag{36}$$

In contrast to Eq. (13) for the stagnation point, Eq. (36) does not depend on the Rayleigh number. This is a consequence of assuming a constant friction factor in the analysis. A more complete solution allowing f = f(Re) would implicitly involve the Rayleigh number. Only numerical solutions are available in this latter case, as reported by Alpert (23, 24).

During the present investigation, the values for the empirical constants suggested by Alpert (23, 24) have been employed. These quantities are summarized in Table 1. Various values of friction factor will be considered in the following.

Table 1. Parameter Values for Ceiling Jet[a]

Parameter	Value (24)
E_p	0.12
E	0.12
β'^2	1.35
γ^2	1.00
Ri_e	0.0196
$\bar{h}_e$	0.0399
$\bar{r}_e$	0.169

[a]Values for E_p and β'^2 based on Rouse, et al (32)

4. Results and Discussion

Methanol, ethanol, 1-propanol and n-pentane were employed as test fuels. Table 2 lists the physical properties of these materials used

Table 2

PHYSICAL PROPERTIES OF FUELS[a]

Property	Methanol	Ethanol	Propanol	Pentane
Molecular Weight	32.04	46.07	60.08	72.14
Boiling Point (K)	337.7	351.5	370.4	309.3
Heat of Vaporization (kJ/kg)[b]	1226	880	788	357
C_p (kJ/kg-K)[b]	1.37	1.43	1.46	1.71
Q_c (mJ/kg-mole)[c]	675	1278	1889	3270

[a]Ambient conditions: $\nu_\infty = 15.3 \times 10^{-6}$ m^2/s, $\mu_\infty = 18.1 \times 10^{-6}$ Ns/m^2, $C_p = 1.005$ kJ/kg-K

[b]Value for the fuel at the boiling temperature

[c]Lower heating value of the fuel at 298 K

to reduce the data. Property values were obtained from Refs. 35-37. All data is summarized in the Appendix.

In the following, the strength of the fire source is frequently represented by the heat generation rate. This quantity was computed from the mass burning rate, as follows:

$$\dot{Q} = \dot{m}_F \, Q_c \tag{37}$$

The use of Eq. (37) to estimate the energy content of the plume neglects heat losses by radiation, which for paraffin hydrocarbons is typically 20% of the total heat generation rate (38).

4.1 Flow Visualization

Figure 4 is a photograph of a turbulent n-pentane fire impinging on an unconfined ceiling. Experimental conditions involved H = 214 mm, D = 91 mm (square) and $\dot{Q}$ = 7.54 kW. The luminous region tends to approach the ceiling near the flame tip, similar to observations of wall fires (16). The flames do not appear to actually return to the ceiling, as required by thin diffusion flame theories, due to wall quenching.

Figure 5 illustrates shadowgraphs of a turbulent 1-propanol fire. The experimental conditions involved H = 165 mm, D = 18 mm and $\dot{Q}$ = 0.2 kW. The shadowgraph arrangement was similar to that used in earlier work on wall fires (12). The bottom figure shows the burning wick, the middle figure shows the impingement region and the top figure is an illustration of the ceiling jet region. The flow is laminar, with some pulsations, near the fuel bed; however, the upper portions of the plume and the ceiling layer are turbulent. Fairly large coherent structures can be observed in the turbulent portions of the flow. However, these structures do not exhibit the regularity observed near the source of turbulent shear layers (39).

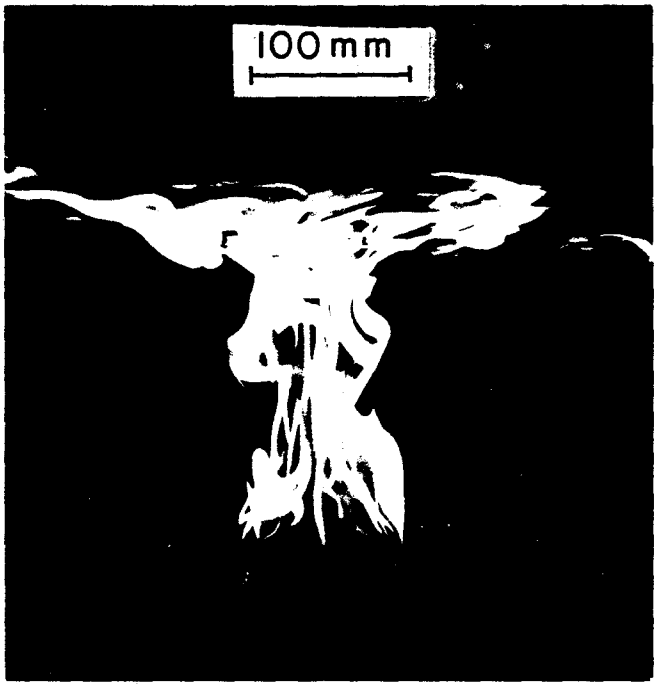

Fig. 4 Photograph of an n-pentane fire impinging on an unconfined ceiling. H = 214 mm, D = 91 mm (square), Q = 7.54 kW.

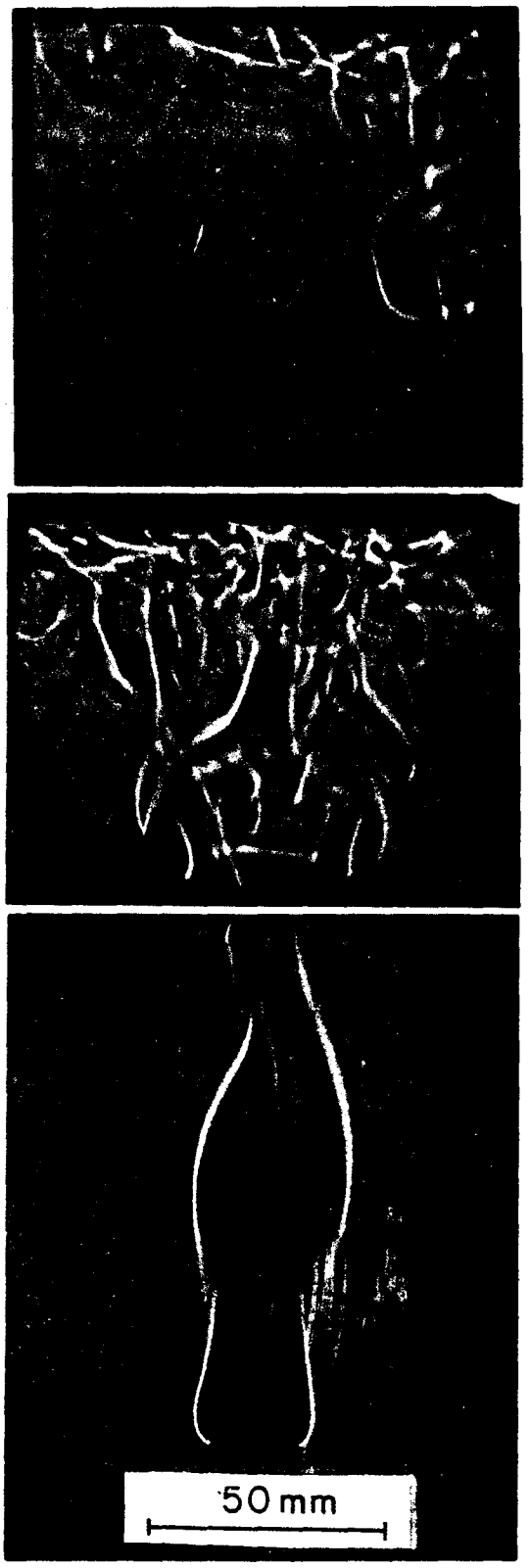

Fig. 5 Shadowgraph of a Turbulent Propanol Fire Plume Impinging on an Unconfined Ceiling. H = 165 mm, D = 18 mm, Q = 0.2 kW.

Structures with greater regularity are observed with laminar plumes. Figure 6 is an illustration of shadowgraphs for this case. The experimental conditions are H = 75 mm, D = 51 mm and $\dot{Q}$ = 0.8 kW. The order of the figures is the same as Fig. 5. In this case, an array of vortices propagates along the ceiling, which is more similar to the large scale structures observed in Ref. 39 for shear layers.

4.2 Flame Height

Figure 7 is an illustration of the correlation of flame height data with no ceiling present. The results are correlated according to Eq. (2), following Steward (29). Other data shown on the plot are due to Thomas, et al (26) for wood cribs, Kosdon, et al (28) for vertical cylinders, and Steward (29) for gas jets.

Using the method of least squares regression the following correlation of the present data was obtained:

$$H_f/D = 10.96\ N_{CO}^{0.211} \tag{38}$$

The power of N_{CO} in Eq. (38) is quite close to the predicted power given by Eq. (2). The present flame height measurements yielded generally lower values than the other investigators. Experimental technique contributes to these discrepancies, since photographic height determinations tend to be biased toward the maximum height of the flame. The degree of flame luminosity is also a factor, e.g. methanol, which forms little soot, generally exhibits the lowest values of H_f/D at a given value of N_{CO}. The characteristics of the source are also a factor, particularly for the low values of H_f/D encountered during the present tests.

4.3 Flame Length Along Ceiling

The experimental results indicated that the free flame height and the length of an impinging flame along a ceiling were related. This

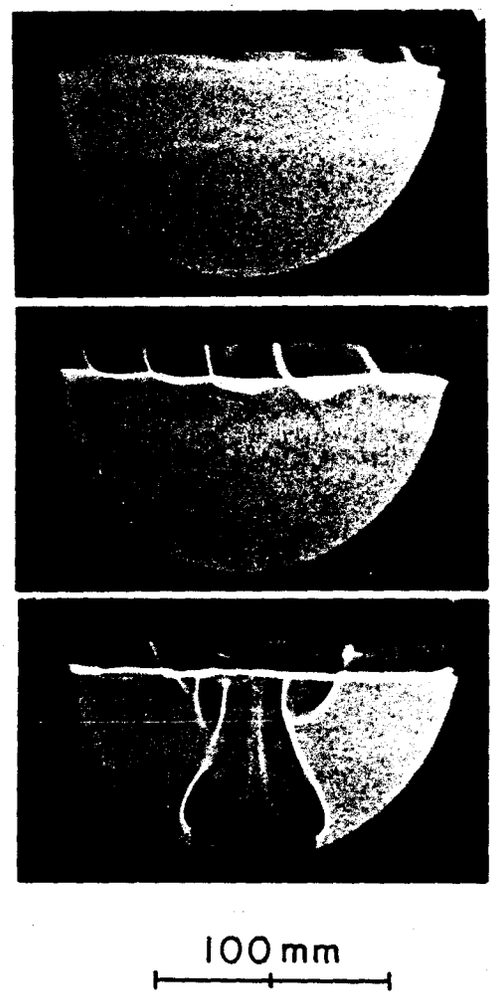

Fig. 6 Shadowgraph of a Laminar Propanol Fire Impinging on an Unconfined Ceiling. H = 75 mm, D = 51 mm, Q = 0.8 kW.

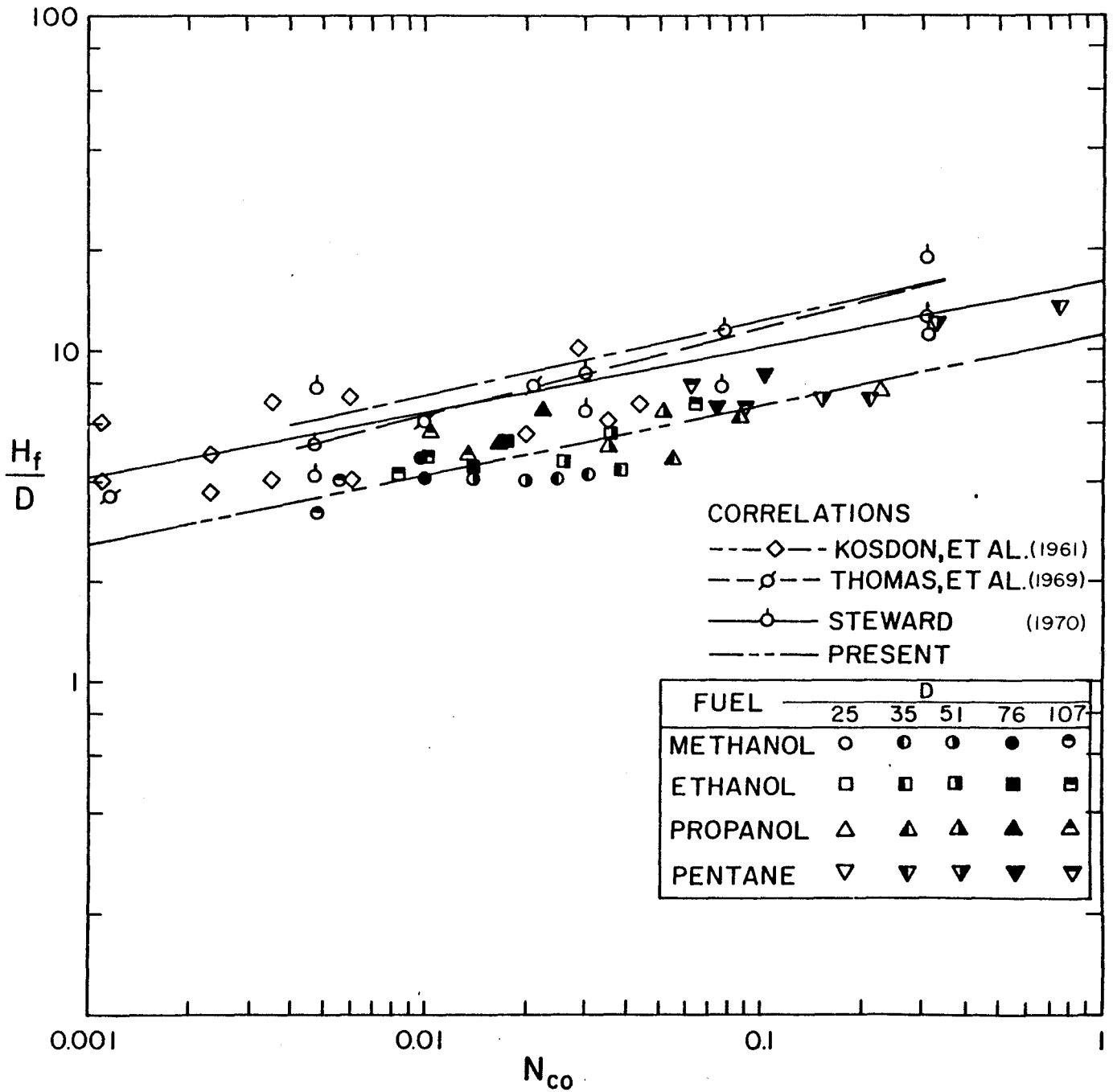

Fig. 7 Free Flame Heights.

correlation is illustrated in Fig. 8. The results consider both confined and unconfined ceilings. In order to facilitate observations, the floor plate of the apparatus, Fig. 1, was removed for these tests.

The uppermost line on Fig. 8, represents the condition where the total length of the flame, when it impinges on the ceiling, is equal to its free flame height, $H_f = H + H_R$, or

$$H_R/D = (H_f - H)/D \tag{39}$$

In general, the measured radial spread is smaller than the value given by Eq. (39). Correlation of the data for an unconfined ceiling yields

$$H_R/D = 0.502[(H_f - H)/D]^{0.957} \tag{40}$$

while the correlation for a confined ceiling is

$$H_R/D = 0.692[(H_f - H)/D]^{0.887} \tag{41}$$

The radial flame spread is larger for the confined ceilings due to the reduced oxygen concentrations in the stratified ceiling layer. The radial spread tends to increase as the length of the wall is increased with the increase in the range 20-40% for the present tests. Since the floor of the apparatus was removed, burning could still be sustained when the ceiling and wall heights were the same, since combustion air could still be entrained from below the fire source position. If the floor were present, lack of ventilation would undoubtedly modify the results although this was not examined during the present experiments.

4.4 Ceiling Heat Flux

Figure 9 is an illustration of the heat flux at the stagnation

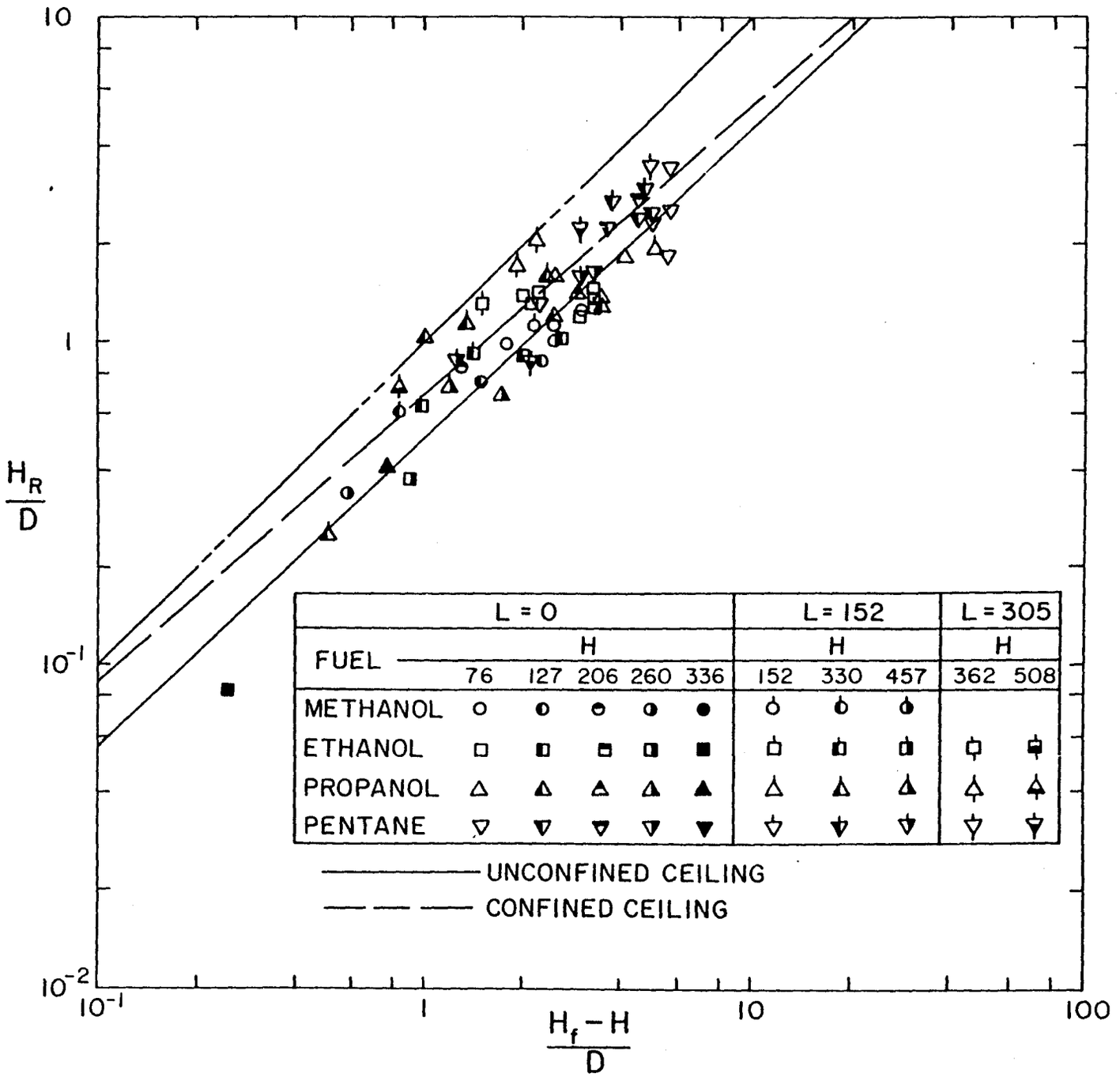

Fig. 8 Flame Lengths along a Ceiling.

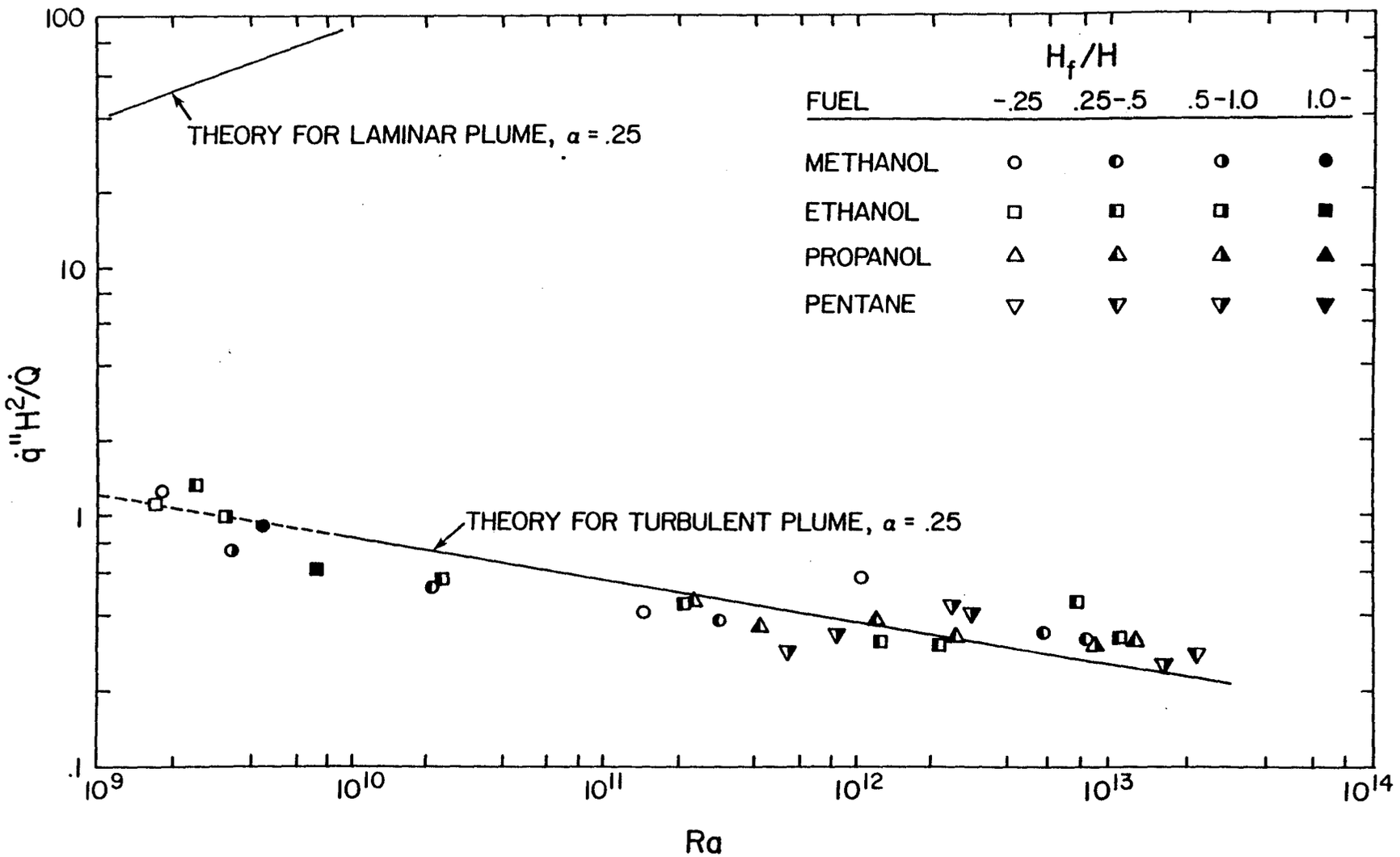

Fig. 9 Stagnation Point Heat Transfer Rates for Plume Impingement on an Unconfined Ceiling.

point as a function of fuel type, H_f/H, and Ra. The measurements are compared with the theoretical correlation given by Eq. (13). The results can be correlated reasonably well in this manner, even for flames that are just impinging on the ceiling, $H_f/H = 1$. Variation of fuel type exerts little influence on the results, over the present test range.

The theoretical expression, Eq. (13), can be fitted to this data by choosing $\alpha = 0.25$ and $F(H/D) = 1$ (the two factors cannot be separated without an independent measurement of dv_e/dr so that Eq. (6) can be evaluated). This yields the following expression for the heat flux for $H_f/H \leq 1$ (results from Fig. 8 indicate the correlation is adequate for somewhat larger values of free flame height, e.g., $H_f/H < 1.5$) and $10^9 < Ra < 10^{14}$:

$$\dot{q}''H^2/\dot{Q} = 31.21\ Pr^{-3/5}Ra^{-1/6} \tag{42}$$

It is of interest to compare the present heat fluxes for impinging plumes with results for impinging jets. Donaldson, et al (30) begin their analysis with a laminar heat flux expression slightly different than that of Sibulkin (31), as follows:

$$\dot{q}''_{lam} = \frac{C_p}{(2Pr)^{1/2}} \left[\rho\mu \frac{dv_e}{dr})_{r=0}\right]^{1/2}(T_e - T_w) \tag{43}$$

Substituting Eqs. (6) and (7) into Eq. (8) yields the following expression for the stagnation point heat flux of a turbulent jet:

$$\dot{q}'' = (2Pr)^{-1/2}[\rho\mu\alpha w_c/r_{1/2}]^{1/2}C_p(T_e - T_w)F(H/D) \tag{44}$$

Equation (44) is very similar to Eq. (8) which was derived for plumes. The differences involve a slightly different power for the Prandtl

number and a relatively small change in the constant. Since plume velocities are controlled by their buoyancy content, w_c and $(T_e - T_w)$ are related for plumes, cf Eqs. (14)-(16). This is not the case for jets; therefore, we can directly compare the heat transfer characteristics of impinging plumes and jets by considering each to have the same w_c, $(T_e - T_w)$ and $r_{1/2}$. Taking the ratio of Eq. (44) to Eq. (8) in this case yields:

$$\dot{q}''_{jet}/\dot{q}''_{plume} = (\alpha^{1/2}F(H/D))_{jet}/(\alpha^{1/2}F(H/D))_{plume} \tag{45}$$

The measurements for the impinging jets and plumes are compared in Table 3. A startling feature of this result is that for comparable conditions, the heat flux of the impinging jet is 2-4 times greater

Table 3 Comparison of Turbulent Impinging Jets and Plumes at the Stagnation Point

	Jet	Plume
Source	Donaldson, et al (30)	Present Study
α	1.13	0.25[a]
F(H/D)	1.4-2.2	1.0[a]
H/D	6-30	2.3 - 21.2
$(w'/w)_e$	0.12-0.22	0.24-0.28[b]
$r_{1/2}/H$	0.091	.112[b], 0.085[c]
$\dot{q}''_{jet}/\dot{q}''_{plume}$	2.6 - 4.2	

[a]Determined by assuming F(H/D) = 1

[b]Measured by George, et al (38), $8 \leq x/D \leq 16$

[c]Measured by Rouse, et al (32)

than that of the impinging plume. In most other respects, the flows are rather similar, e.g. width with respect to distance from the source, turbulence intensity, etc. Several factors could contribute to this behavior. In the present experiments, $\dot{Q}$ was evaluated from the total combustion energy of the fuel, neglecting radiation. Therefore, the actual $\dot{Q}$ in the plume may be somewhat lower than the present estimation, and use of the correct value would tend to increase the heat flux parameter for plume impingement (results considered later, however, indicate plume characteristics are represented reasonably well by the present approach). We also assume that the heat of combustion is released at the source, when Eqs. (9)-(11) are employed to evaluate w_c and $(T_e - T_w)$. Actually, the heat is released over a significant fraction of the ceiling height in the present experiments, tending to reduce plume velocities since the complete buoyant force only acts over a portion of the ceiling height. This would also tend to reduce the stagnation point heat flux, cf Eq. (8).

There is also the possibility of fundamental differences in the impingement processes of plumes and jets. Until velocity measurements are available for the impinging plume it is impossible to determine whether the reduced heat flux is due to lower values of α, i.e. lower rates of acceleration of the flow near the stagnation point, or a smaller effect of the turbulence level on thermal boundary layer near the wall. The influence of flow stratification through the Richardson number, could be a factor in both effects. Clearly, further work will be required in order to more fully understand the impingement process of plumes and their relation to jet flows.

The theoretical expression for stagnation point heat flux for a

laminar plume, Eq. (17), is also illustrated on Fig. 9. For lack of other information, the turbulent value of α has been used to plot the correlation. The predicted heat flux for a laminar plume is much higher than the turbulent plume, since laminar plumes mix more slowly with the ambient fluid. This results in higher values of temperature and velocity in laminar plumes which increases the heat transfer rate at the stagnation point. The present fire sources were turbulent for Ra as low as 2×10^9, which is somewhat lower than the transition criteria given by Yih (33) of 9×10^9, for weaker sources. Therefore, the potentially interesting jump in the heat flux in the transition region was not observed during the present investigation.

Figure 10 is an illustration of the effect of flame height on the stagnation point heat flux for unconfined ceilings. For values of H_f/H in the range 0 - 1.5, the stagnation point heat flux is independent of H_f/H. From the results of Fig. 8, or Eq. (40), this corresponds to $0 \leq H_R/H \leq 0.25$, which includes conditions where the flame has spread a significant distance along the ceiling. For larger values of H_f/H or H_R/H, the stagnation point heat flux decreases. This is due to the fact that the cool, unburned core of the plume reaches the ceiling, reducing the temperature levels of the gas stream that contacts the stagnation point.

Figure 11 is an illustration of the variation of ceiling heat flux with radial distance from the stagnation point. These results are for unconfirmed ceilings. In addition to the present data, measurements are also included from the work of Alpert (23) and Zukoski, et al (19). Two sets of theoretical curves are shown on the figure. The first set,

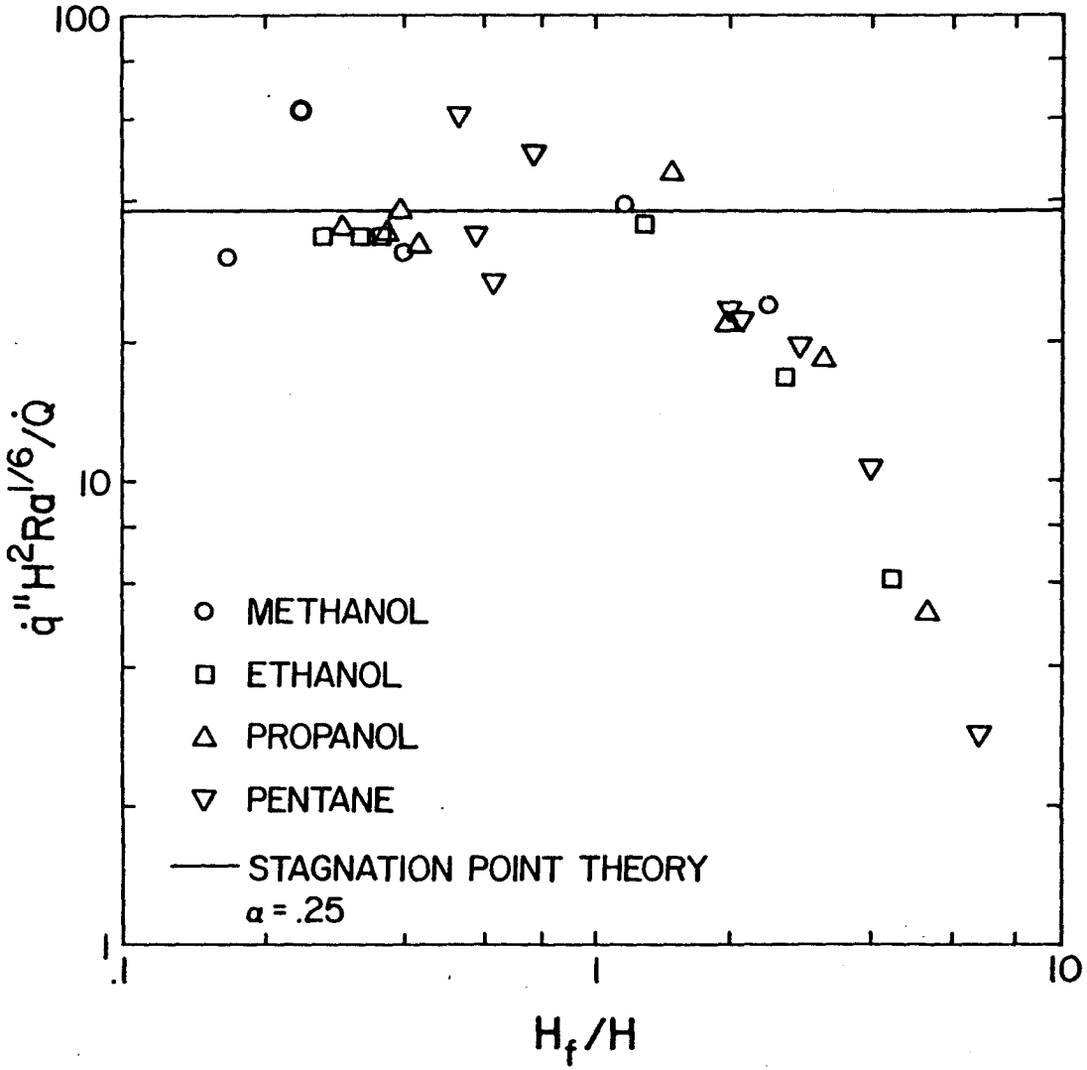

Fig. 10 Effect of Flame Impingement on Stagnation Point Heat Transfer Rates on an Unconfined Ceiling.

for the region of the stagnation point, is obtained from Eq. (42), using two values of Ra that span the range of the data shown on the figure. The second set of curves, for $r/H > 0.2$, employs Alpert's (23, 24) numerical solution for values of f=0.02 and 0.04. The other parameters used in this computation are summarized in Table 1.

The scatter of the data on Fig. 11 is appreciable. Clearly all relevant factors are not considered by these simple correlation schemes. In the stagnation region, the use of Eq. (42) directly illustrated in Fig. 8, reduces the scatter since the effect of Rayleigh number is included. Employing the Rayleigh number correction for $r/H > 0.2$, however, increases the scatter in that region. The best current estimation for the heat flux involves employing Eq. (42) for the stagnation region, $r/H < 0.2$; and fitting the data for $r/H > 0.2$, viz. The use of Eq.

$$\dot{q}''/\dot{Q}H^2 = 0.353Pr^{-2/3}\{1 + 18.87[(r/H)^2 - 0.0287]\}^{-(1 + .059Pr^{-2/3})} \quad (46)$$

(36) tends to overestimate the reduction of heat flux with radial distance.

The effect of flame impingement on the ceiling is illustrated in Fig. 12. Similar to Fig. 11, the theoretical expressions are also shown on the figures. In the region of the stagnation point, flames which spread a significant distance along the ceiling, exhibit reduced heat transfer rates. This finding was illustrated explicitly in Fig. 10. For values of $r/H > 0.2$, however, significant differences from the results for non-impinging flames are not observed. This was the case for H_R/H up to 0.6, the largest value considered. For this range of conditions, Eq. (46) is still adequate for estimating the heat flux resulting from impinging flames.

Figure 13 is an illustration of heat flux measurements with confined

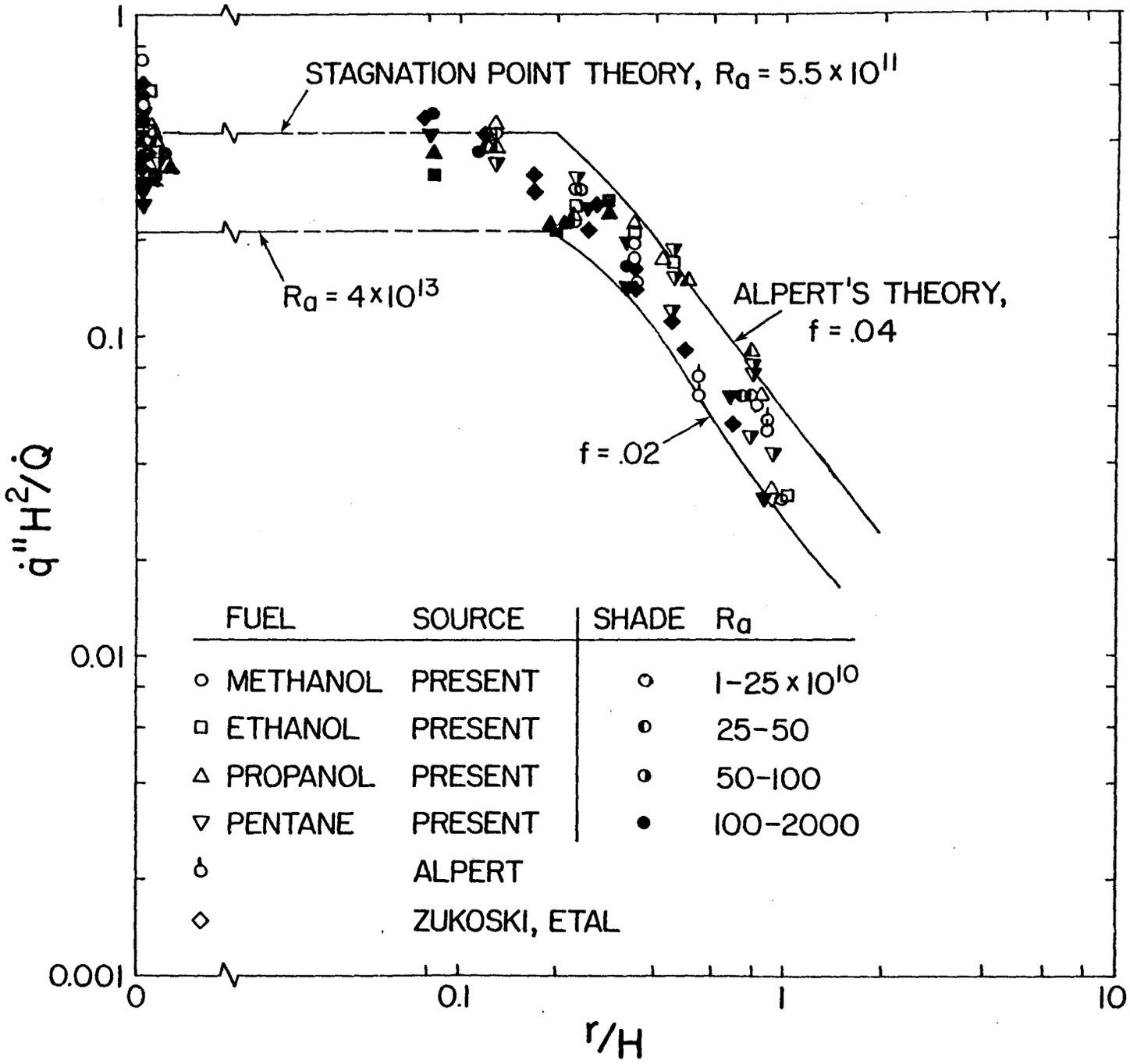

Fig. 11 Ceiling Heat Fluxes for Plume Impingement on an Unconfined Ceiling.

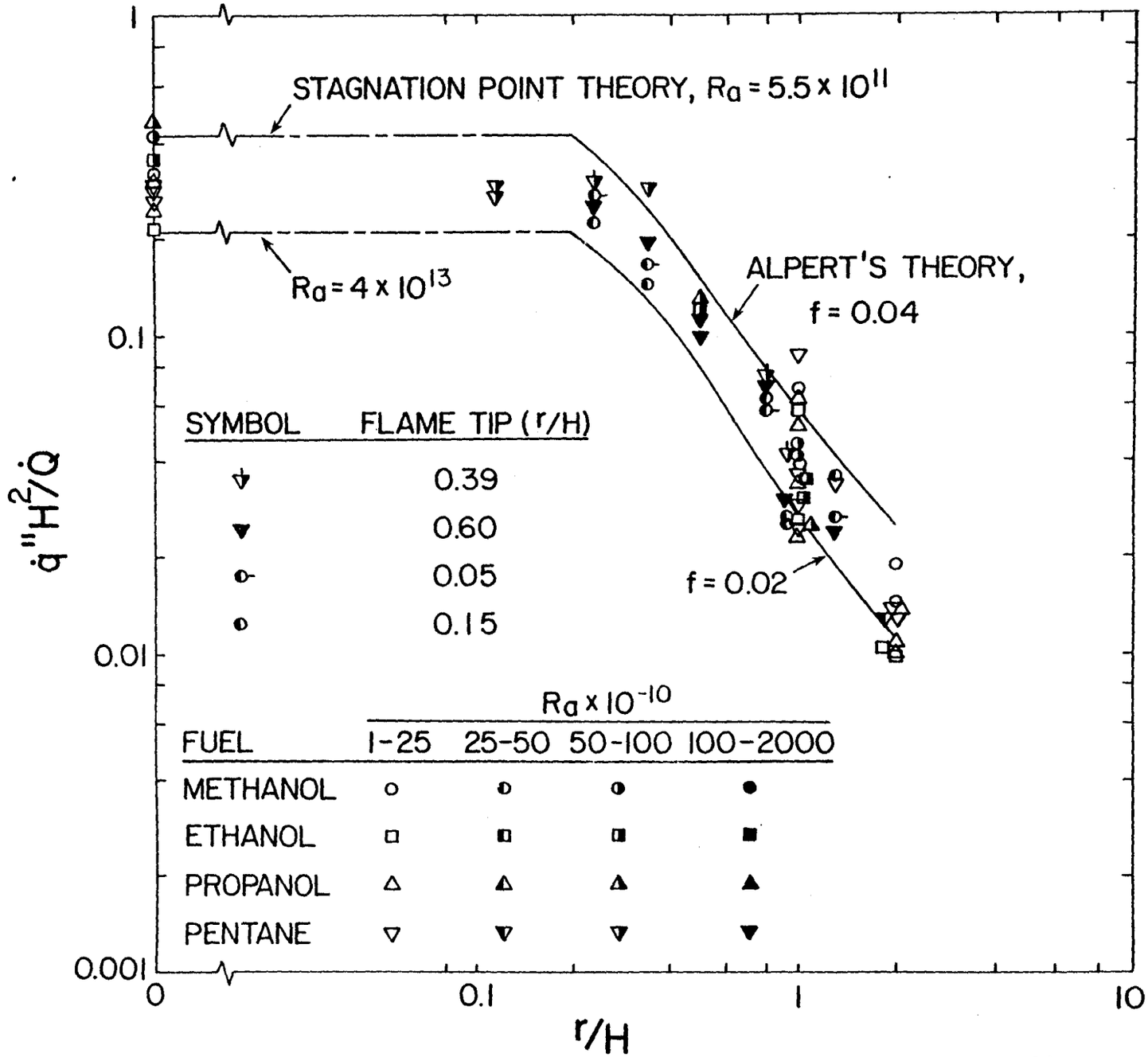

Fig. 12 Ceiling Heat Fluxes for Flame Impingement on an Unconfined Ceiling.

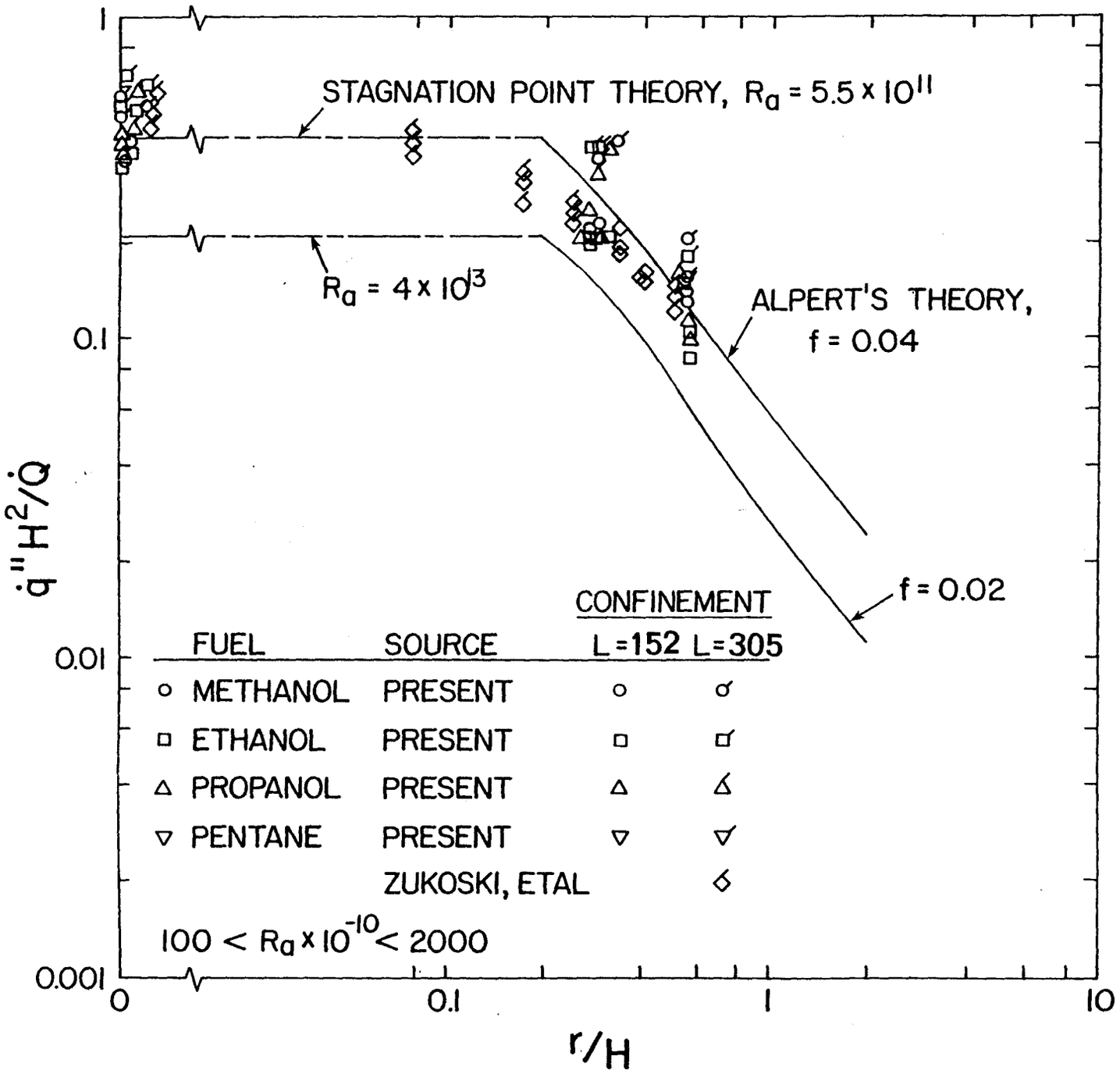

Fig. 13 Ceiling Heat Fluxes for Plume Impingement on a Confined Ceiling.

ceilings. Two degrees of confinement were considered, comprising $L = 152$ and 305 mm. The heat fluxes are higher for confined ceilings, and tend to increase as the degree of confinement increases. The correlations provided by Eqs. (42) and (46) underestimate this data somewhat, but at least provide a reasonable first estimation of the results. Additional study will be required to fully resolve the effect of confinement on the ceiling heat flux.

4.5 Mean Temperature Distributions

Mean temperature distributions for both unconfined and confined ceilings are illustrated in Figs. 14 and 15. For these tests, $D = 20$ mm, $H = 695$ mm, $\dot{Q} = 246\text{-}250$ kW, $H_f = 89\text{-}102$ mm and methanol was used as the test fuel. The curtain wall, Fig. 15, was 610 mm in diameter and had a length of 241 mm.

During these tests, flow instabilities near the source would occasionally cause the center of the temperature profile to shift from the geometrical center of the wick; however, shift distances were no greater than 10 mm. Even though the ceiling was insulated, and allowed to reach a steady condition, there was still some heat loss from the ceiling; therefore, temperature profiles in the ceiling jet show a slight reduction near the surface of the ceiling. Since the flame height was relatively low, maximum temperatures are less than 66C above the ambient temperature; therefore, the measurements are in the weakly buoyant region of the flow.

For the unconfined ceiling, Fig. 14, temperatures within the plume and the ceiling jet decline continuously with increasing distance from the source. For the confined ceiling, Fig. 15, temperatures within the ceiling

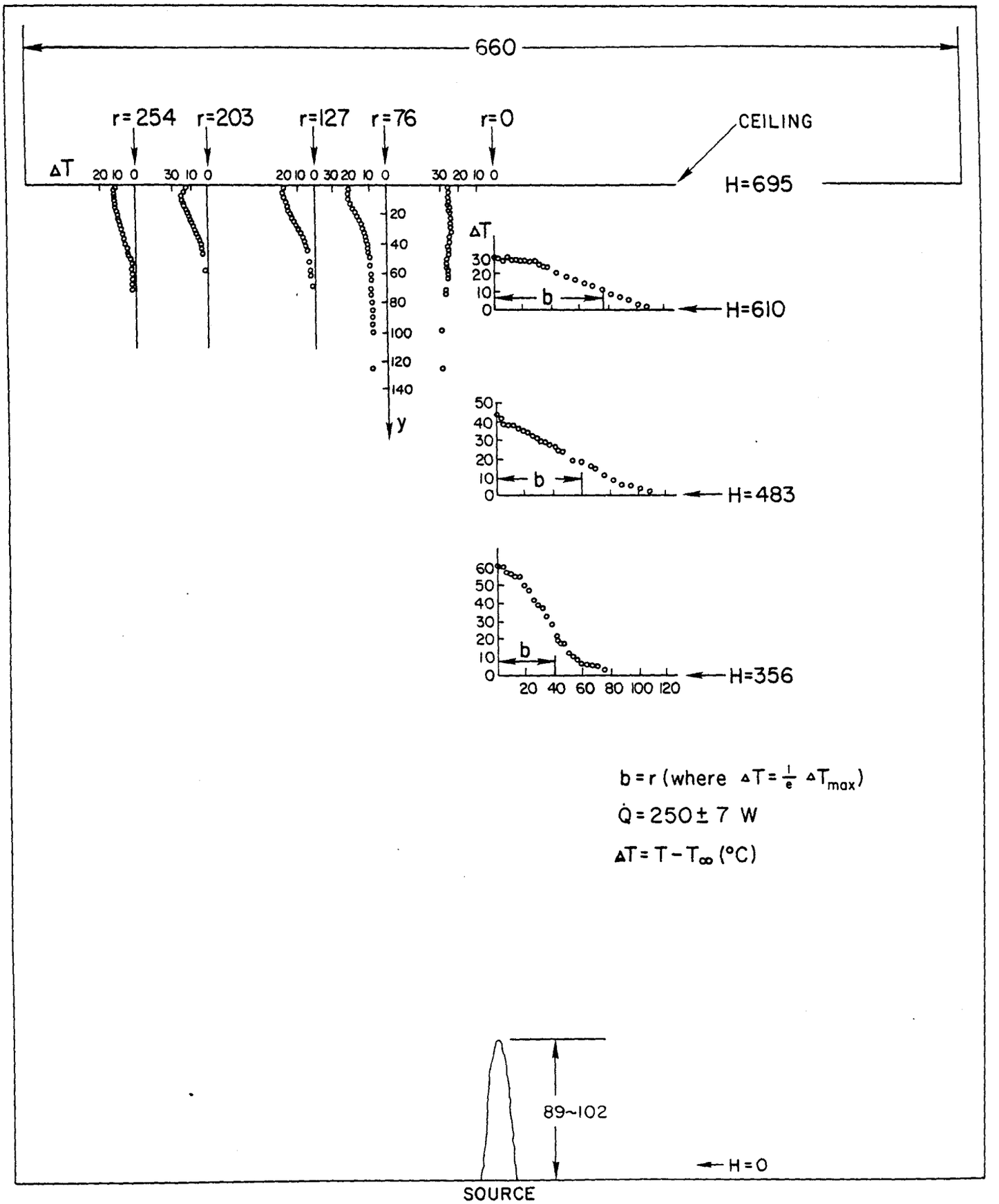

Fig. 14 Temperature Distributions in the Plume and the Ceiling Jet for an Unconfined Ceiling.

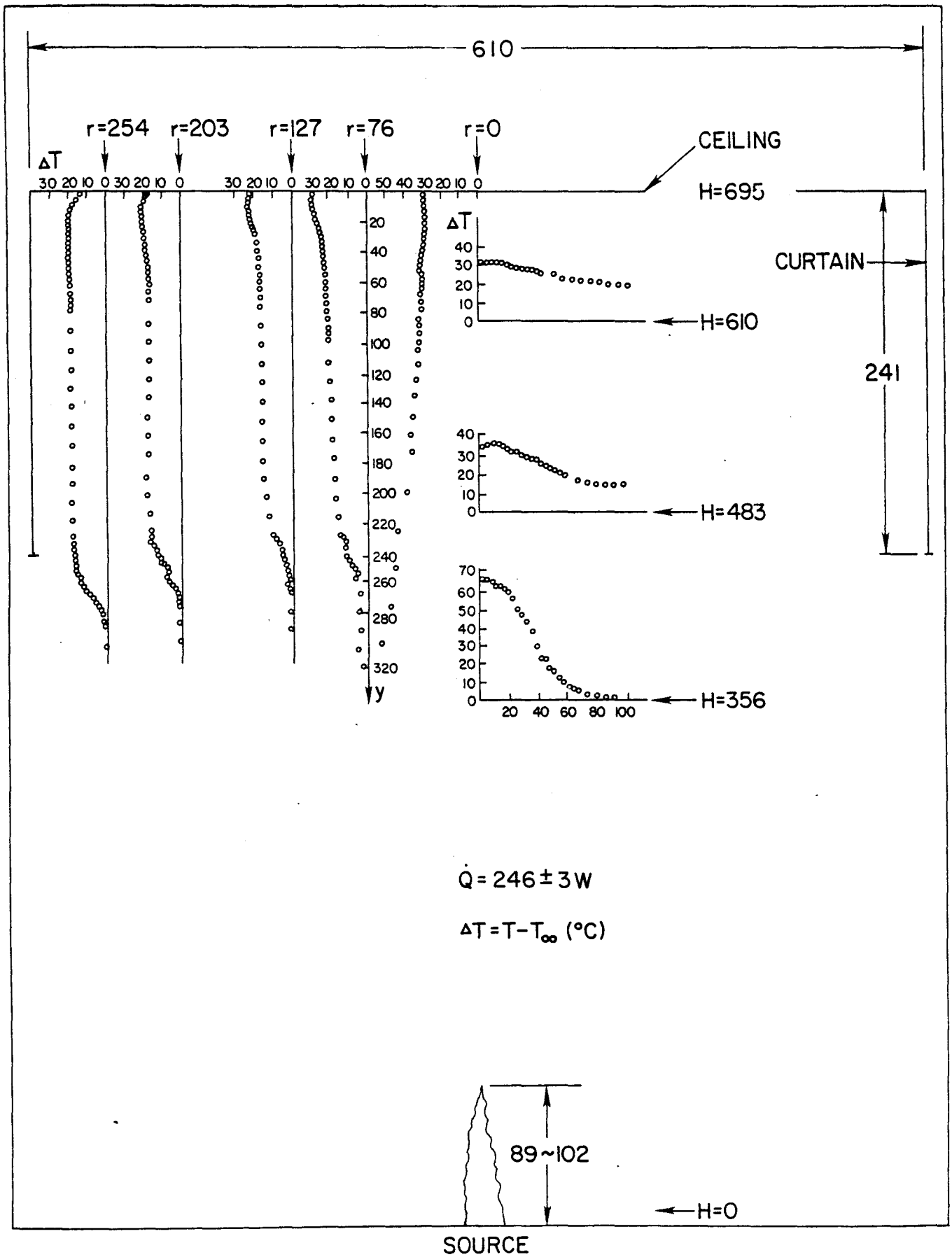

Fig. 15 Temperature Distributions in the Plume and the Ceiling Jet for a Confined Ceiling.

layer are relatively uniform and the temperature disturbance due to the ceiling jet is less well-defined than for the unconfined ceiling. The lower edge of the ceiling layer slants downward when passing from the plume position toward the curtain wall, reaching a depth approximately 40 mm below the lower edge of the curtain wall for this test condition. This effect is due to the passage of relatively cool air near the edge of the plume into the ceiling layer.

With this data available, it is of interest to compare the results with various theoretical predictions for the plume, ceiling jet, ceiling layer, etc. These comparisons are described in the following.

Plume. Plume profiles can be correlated in the following form:

$$wzRa^{-1/3}/\nu = C_w \exp[-(r/\ell_p z)^2] \tag{47}$$

$$g\beta(T - T_\infty)z^3 Ra^{-2/3}/\nu^2 = C_T \exp[-(r/\beta'\ell_p z)^2] \tag{48}$$

where the Rayleigh number in these equations is the same as Eq. (11), except that the height, z, above the source of the plume replaces the ceiling height H. The constants appearing in Eqs. (47) and (48) have been measured by Rouse, et al (32), George, et al (38) and Yokoi (34). Their values are summarized in Table 4. Due to the difficulties in accurately measuring velocities and temperatures in plumes, the constants from the three investigations differ and additional study will be required to resolve these differences.

The temperature correlation given by Eq. (48) is compared with the present measurements in Table 5. The present measurements agree reasonably well with the earlier studies, particularly those of Rouse,

Table 4

PLUME PROFILE CONSTANTS

Source	C_w	C_T	δ	β'	$\pi C_w \delta^2$
Rouse, et al (32)	4.7	11.0	.102	1.17	.154
George, et al (38)	3.4	9.0	.135	.92	.195
Yokoi (34)	3.8	9.1	.125	1.15	.187

Table 5

SUMMARY OF PLUME CHARACTERISTICS[a]

z (mm)	$\dot{Q}$ (W)	ΔT_c (K)	Ra X 10^{-11}	$g\beta\Delta T_o z^3 Ra^{-2/3}/\nu^2$	r/z ($\Delta T/\Delta T_{mm} = e^{-1}$)
Unconfined Ceiling					
356	243	61.9	2.38	10.1	.113
483	245	43.5	4.42	11.0	.133
610	246	28.2	7.07	11.2	.127
Confined Ceiling					
356	245	65.7	2.40	10.8	.113
483[b]	245	37.2	4.42	10.2	--
610[b]	242	32.0	6.96	13.0	--
Rouse, et al (32)				11.0	.119
George, et al (38)				9.0	.124
Yokoi (34)				9.1	.143

[a]Properties taken as follows: $\rho = 1.18$ kg/m^3, $\nu = 15.3 \times 10^{-6}$ m^2/s $C_p = 1005$ J/kgK, $\beta = 3.36 \times 10^{-3}$ K^{-1}, $g = 9.806$ m/s^2

[b]This portion of plume is in ceiling layer.

et al (32). This implies that the constants, and the estimation of plume properties, used to develop Eqs. (13) and (42) are reasonable. During the confined plume measurements, the two highest positions for plume measurements are within the ceiling layer and Eq. (48) does not apply. Nevertheless, we see that values of the maximum temperature parameter are comparable to the other cases.

Ceiling Jet. The results for the unconfined ceiling can be compared with Alpert's model (23, 24). Similar to the heat transfer results, we assume f = .03 will provide the best fit of the data. Substituting parameter values from Table 1 into Eqs. (21)-(35) yields the following expressions for ceiling jet quantities:

$$\ell/H = 5.38 \times 10^{-3}\ \phi/(r/H) \tag{49}$$

$$vHRa^{-1/3}/\nu = 5.14\ \phi^{-.529}\ \exp[-(y/\ell)^2] \tag{50}$$

$$g\beta\Delta TH^3Ra^{-2/3}/\nu^2 = 9.18\ \phi^{-(.471\ +\ .059\ Pr^{-2/3})}\exp[-(y/\ell)^2] \tag{51}$$

where

$$\phi = 1 + 18.87[(r/H)^2 - 0.0287] \tag{52}$$

Since $\gamma = 1$, from Table 1, $\ell = \ell_T$ for this correlation.

Ceiling jet characteristics obtained from Eqs. (49)-(51) are compared with the present measurements, illustrated in Fig. 14, in Table 6. Similar measurements by Zukoski, et al (25) are also summarized in the table.

The two sets of measurements are in reasonably good agreement with each other, at comparable values of r/H. The theory generally underestimates

Table 6

SUMMARY OF CEILING JET CHARACTERISTICS[a]

r/H	$\dot{Q}$ (W)	ΔT_{max} (K)	Ra	ℓ_r/H		$g\beta\Delta T_{max}H^3/Ra^{2/3}\nu^2$	
				Measured	Predicted	Measured	Predicted
Present Data, H = 695 mm							
.109[b]	257	23.1	9.59×10^{11}	--	--	11.1	11.3
.183	253	19.4	9.44×10^{11}	.053	.032	9.5	8.8
.292	248	14.3	9.26×10^{11}	.054	.038	7.1	6.2
.366	255	12.2	9.52×10^{11}	.065	.044	6.0	5.1
Zukoski, et al (25), H = 813 mm							
.219	1170	37	5.98×10^{12}	.048	.034	8.5	7.8
.312	1170	30	5.98×10^{12}	.044	.049	6.9	5.8
.469	1170	22	5.98×10^{12}	.050	.053	5.0	4.0
.312	1530	40	7.82×10^{12}	.044	.040	7.6	5.8
.469	1530	27	7.82×10^{12}	.059	.053	5.1	4.0

[a]Properties the same as Table 5.

[b]Located in turning region, ℓ_t/H not relevant.

the maximum temperature in the ceiling jet by about 20%. The theory also tends to underestimate the width of the ceiling layer. The general trends of the theory, however, conform with the measurements.

Applying the same approach to the ceiling layer for a confined plume should also be possible, if the characteristics of the impinging plume can be defined. Work is currently in progress in order to allow this extension.

Ceiling Layer. If we exclude heat losses from the ceiling layer, the average temperature in this region should be the same as the average temperature of the plume when it strikes the lower edge of the layer. Expressions for the mass flow rate and average temperature of the plume are as follows:

$$\dot{m} = \int_{o}^{\infty} \rho w 2\pi r dr \tag{53}$$

$$\dot{Q} = \dot{m}\, C_p\, \overline{\Delta T} \tag{54}$$

Substituting Eq. (47) into Eq. (53), completing the integration, and then substituting the result into Eq. (54), yields the following expressions for the mass flow rate and average plume temperature:

$$\dot{m}/\rho\nu z Ra^{1/3} = \pi C_w \ell_p^{\,2} \tag{55}$$

$$g\beta\overline{\Delta T} z^3/\nu^2 Ra^{2/3} = (\pi C_w \ell_p^{\,2})^{-1} \tag{56}$$

The right hand side of these equations varies, depending upon the source of the measurements, as shown in Table 4.

The present measurements can be compared with Eq. (56), if we also

ignore heat loss from the ceiling layer. Examination of Figure 15 indicates that the lower edge of the layer is not precisely defined, but is in the range 230-260 mm from the ceiling in the central region near the plume. The appropriate average temperature of the layer is obtained from the region outside the plume, the ceiling jet, and the lower edge of the ceiling layer. Predictions and the measurement are compared in Table 7. The measured temperature defect is 15-30% lower than all the predictions, probably due to heat losses.

Table 7

PREDICTED AND MEASURED CEILING LAYER TEMPERATURES[a]

Ceiling Layer Height (mm)	435	465
Rayleigh Number[b]	3.60×10^{11}	4.11×10^{11}
Predicted ΔT(C)		
Rouse, et al (32)	26	29
George, et al (38)	20	23
Yokoi (34)	21	24
Measured ΔT(C)	18-19	

[a] $\dot{Q}$ = 246 W, H = 695 mm, L = 241 mm, D_c = 610 mm
properties the same as Table 5

[b] Of plume at the point where it reaches the ceiling layer.

References

1. H. W. Emmons, H. E. Mitler, and L. N. Trefethen, "Computer Fire Code III", Home Fire Technical Report No. 25, Harvard University, Cambridge, MA (1978).

2. E. E. Zukoski and T. Kubota, "A Computer Model for Fluid Dynamic Aspects of a Transient Fire in a Two Room Structure", Report under USDC-NBS, Center for Fire Research Grant No. 5-9004, California Institute of Technology, Pasadena, CA (1978).

3. E. E. Smith and M. J. Clark, "Model of the Developing Fire in a Compartment", ASHRAE Trans. 81, Part I, 568 (1975).

4. A. C. Ku, M. L. Doria, and J. R. Lloyd, "Numerical Modeling of Unsteady Buoyant Flows Generated by Fire in a Corridor", Sixteenth Symposium (International) on Combustion, The Combustion Institute, Pittsburgh, PA, 1373 (1977).

5. T. Tanaka, "A Mathematical Model of a Compartment Fire", Second Joint Meeting, U.S.-Japan Panel on Fire Research and Safety, UJNR, Tokyo (1976).

6. J. A. Liburdy and G. M. Faeth, "Fire Induced Plumes Along a Vertical Wall: Part I. The Turbulent Weakly Bouyant Region", Report under USDC-NBS, Center for Fire Research Grant 5-9020, The Pennsylvania State University, University Park, PA (1977).

7. T. Ahmad, E. G. Groff, and G. M. Faeth, "Fire Induced Plumes Along a Vertical Wall: Part II. The Laminar Combusting Plume", Report under USDC-NBS, Center for Fire Research Grant No. 5-9020, The Pennsylvania State University, University Park, PA (1977).

8. T. Ahmad and G. M. Faeth, "Fire Induced Plumes Along a Vertical Wall: Part III. The Turbulent Combusting Plume", Report under USDC-NBS, Center for Fire Research Grant No. 5-9020, The Pennsylvania State University, University Park, PA (1978).

9. J. J. Grella and G. M. Faeth, "Measurements in a Two-Dimensional Thermal Plume Along a Vertical Adiabatic Wall", J. Fluid Mech. 71, 701 (1975).

10. J. A. Liburdy andG. M. Faeth, "Theory of a Steady Laminar Thermal Plume Along a Vertical Adiabatic Wall", Letters in Heat and Mass Transfer 2, 407 (1975).

11. J. A. Liburdy and G. M. Faeth, "An Experimental Investigation of a Turbulent Thermal Plume Along an Isothermal Wall", First Symposium on Turbulent Shear Flows, The Pennsylvania State University Park, PA, Vol. 1, 6.51 (1977).

12. T. Ahmad and G. M. Faeth, "An Investigation of the Laminar Overfire Region Along Upright Surfaces", Trans. ASME, Series C, J. Heat Transfer 100, 112 (1978).

13. E. G. Groff and G. M. Faeth, "Laminar Combustion of Free-Standing Fuel Surfaces", Combustion and Flame 32, 139 (1978).

14. J. A. Liburdy and G. M. Faeth, "Heat Transfer and Mean Structure of a Turbulent Thermal Plume Along a Vertical Isothermal Wall", Trans. ASME, Series C., J. Heat Transfer 100, 177 (1978).

15. J. A. Liburdy, E. G. Groff, and G. M. Faeth, "Structure of a Turbulent Thermal Plume Rising Along a Vertical Isothermal Wall", ASME Paper No. 78-HT-24 (1978).

16. T. Ahmad and G. M. Faeth, "Turbulent Wall Fires", Seventeenth Symposium (International) on Combustion, Leeds, England, August 1978.

17. T. H. Ellison and J. S. Turner, "Turbulent Entrainment in Stratified Flows", J. Fluid Mech. 6, 424 (1959).

18. W. D. Baines and J. S. Turner, "Turbulent Buoyant Convection from a Source in a Confined Region", J. Fluid Mech. 37, 51 (1969).

19. E. E. Zukoski, "Convective Flows Associated with Room Fires", Proceedings of the Annual Conference in Fire Research, National Fire Prevention and Control Administration, U.S. Department of Commerce, pp. B-1 to B-4 (1976).

20. J. Prahl and H. W. Emmons, "Fire Induced Glow through an Opening", Combustion and Flame, Vol. 25, pp. 369-385 (1975).

21. P. H. Thomas, J.F.R.O. Note No. 141, Fire Research Station, Boreham Wood, Herts, England (1955).

22. R. W. Pickard, D. Hird, and P. Nash, J.F.R.O. Note No. 247, Fire Research Station, Boreham Wood, Herts, England (1957).

23. R. L. Alpert, "Fire Induced Turbulent Ceiling-Jet", Technical Report No. 19722-2, Factory Mutual Research Corporation, Norwood, MA (1971).

24. R. L. Alpert, "Turbulent Ceiling-Jet Induced by Large-Scale Fire", Technical Report No. 22357-2, Factory Mutual Research Corporation, Norwood, MA (1974).

25. E. E. Zukoski, T. Kubota, and C. C. Veldman, "Experimental Study of Environment and Heat Transfer in a Room Fire", Technical Report No. 1, Grant No. 5-9004, California Institute of Technology, Pasadena, CA (1975).

26. P. H. Thomas, C. T. Webster, and M. M. Raftery, "Some Experiments on Buoyant Diffusion Flames", Combustion and Flame 5, 359 (1961).

27. A. A. Putnam and C. F. Speich, "A Model Study of the Interaction of Multiple Turbulent Diffusion Flames", Ninth Symposium (International) on Combustion, Academic Press, New York, 867 (1963).

28. F. J. Kosdon, F. A. Williams and C. Buman, "Combustion of Vertical Cylinders in Air", Twelfth Symposium (International) on Combustion, The Combustion Institute, Pittsburgh, PA, 253 (1969).

29. F. R. Steward, "Prediction of the Height of Turbulent Diffusion Buoyant Flames", Comb. Sci. and Tech. 2, 203 (1970).

30. C. DuP. Donaldson, R. S. Snedeker, and D. P. Margolis, "A Study of Free Jet Impingement: Part 2. Free Jet Turbulent Structure and Impingement Heat Transfer", J. Fluid Mech. 45, 477 (1971).

31. M. Sibulkin, "Heat Transfer Near the Forward Stagnation Point of a Body of Revolution", J.Aero. Science 19, 570 (1952).

32. H. Rouse, C. S. Yih, and H. W. Humphreys, "Gravitational Convection from a Boundary Source", Tellus 4, 201 (1952).

33. C. S. Yih, "Free Convection Due to Boundary Sources", Fluid Models in Geophysics, Proceedings of the First Symposium on the Use of Models in Geophysical Fluid Dynamics, The John Hopkins University, September 1-4, pp. 117-133 (1953).

34. S. Yokoi, "Study on the Prevention of Fire Spread Caused by Hot Upward Current", Report No. 34, Building Research Institute, Japanese Government, November 1960.

35. R. H. Perry and C. H. Chilton, Chemical Engineer's Handbook, McGraw-Hill Book Co., New York (1973).

36. R. E. Bolz and G. L. Tuve, Handbook of Tables for Applied Engineering Science, The Chemical Rubber Co., Cleveland, Ohio (1970).

37. F. D. Rossini, Selected Values of the Physical and Thermodynamic Properties of Hydrocarbons and Related Compounds, A.P.I., Carnegie, (1953).

38. W. K. George, Jr., R. L. Alpert, and F. Tamanini, "Turbulence Measurements in an Axisymmetric Buoyant Plume", Technical Report FMRC Serial No. 22359-2, Factory Mutual Research Corporation, Norwood, MA (1976).

39. G. H. Markstein, "Scaling of Radiative Characteristics of Turbulent Diffusion Flames", Sixteenth Symposium (International) on Combustion, The Combustion Institute, Pittsburgh, 1407 (1976).

40. A. Roshko, "Structure of Turbulent Shear Flows: A New Look", AIAA J 14, 1349-1357 (1976).

APPENDIX

TABULATION OF DATA

Table A-1. FREE FLAME HEIGHT DATA

D (mm)	$\dot{Q}$ (W)	H_f (mm) min.	H_f (mm) max.
n-Pentane			
35	778	229	280
35	1489	432	508
51	1620	330	381
51	2510	559	660
76	4190	610	737
107	6610	762	889
107	7890	610	762
Methanol			
35	357	127	152
35	373	130	180
51	640	178	230
51	725	178	229
76	1340	279	381
76	1380	330	381
107	2260	330	368
107	2340	381	457

Table A-1. FREE FLAME HEIGHT DATA
(continued)

D (mm)	$\dot{Q}$ (W)	H_f (mm) min.	H_f (mm) max.
Ethanol			
35	408	140	165
35	491	229	254
51	707	203	254
51	896	254	305
76	1730	356	432
107	2770	406	483
107	3000	483	559
1-Propanol			
35	393	178	203
35	557	203	241
51	786	230	280
51	1050	305	356
76	1640	356	432
76	1900	457	533
107	3290	533	635
107	3310	559	635

Table A-2. FLAME LENGTH ALONG CEILING (NO CURTAIN WALL)

D (mm)	$\dot{Q}$ (W)	H (mm)	H_R (mm) min.	H_R (mm) max.	H_f (avg) (mm)	H_R (avg) (mm)
Methanol						
35	366	76	32	38	138	35
51	620	76	44	57	204	51
51	620	127	25	51	204	38
76	1190	76	76	114	304	95
76	1190	127	63	70	304	66
76	1190	260	0	52	304	26
107	2260	76	108	133	350	120
107	2260	206	51	127	350	89
Ethanol						
35	410	76	40	52	152	46
51	707	76	51	70	229	60
76	1540	76	89	114	356	101
76	1540	127	63	102	356	82
76	1540	260	25	32	356	28
76	1540	336	0	13	356	6
107	2770	76	133	178	444	155
107	2770	206	127	165	444	146

Table A-2. FLAME LENGTH ALONG CEILING (NO CURTAIN WALL)
(continued)

D (mm)	$\dot{Q}$ (W)	H (mm)	H_R (mm) min.	H_R (mm) max.	H_f (avg) (mm)	H_R (avg) (mm)
1-Propanol						
35	360	76	51	63	170	57
35	360	127	25	57	170	41
51	786	76	63	76	254	70
51	786	127	51	70	254	60
76	1640	127	89	108	394	101
76	1640	260	25	79	394	52
76	1640	336	13	51	394	32
107	3290	76	152	229	521	190
107	3290	206	127	178	521	152
n-Pentane						
35	778	76	51	112	254	81
35	778	127	63	92	254	77
51	1620	76	76	108	356	92
76	3460	76	152	229	508	190
76	3460	127	165	209	508	187
76	3460	260	102	146	508	124
76	3460	336	76	121	508	98
107	7890	76	305	406	686	356
107	7890	206	254	330	686	292

Table A-3. FLAME LENGTH ALONG CEILING (CURTAIN WALL)

D (mm)	$\dot{Q}$ (W)	H (mm)	H_R (mm) min.	H_R (mm) max.	H_f (avg)	H_R (avg)
Dc = 610 mm, L = 152 mm						
Methanol						
76	1380	152	76	95	355	85
107	2340	330	51	64	419	57
Ethanol						
76	1820	152	95	102	406	98
76	1820	330	44	51	406	47
107	2920	330	89	108	483	95
1-Propanol						
51	1200	330	0	26	350	13
76	1800	330	76	102	431	89
107	3310	330	140	203	585	171
107	3310	460	64	89	585	76
n-Pentane						
51	2370	330	114	159	521	136
51	2370	460	25	64	521	44
76	4790	330	191	254	685	222
76	4790	460	102	140	685	121
Dc = 610 mm, L = 305 mm						
Ethanol						
107	3060	362	127	152	521	140
1-Propanol						
76	2060	362	114	146	507	130
107	3540	362	178	267	598	222
107	3170	508	51	102	598	76

Table A-3. FLAME LENGTH ALONG CEILING (CURTAIN WALL)
(continued)

D (mm)	$\dot{Q}$ (W)	H (mm)	H_R (mm) min.	H_R (mm) max.	H_f (avg) (mm)	H_R (avg) (mm)
n-Pentane						
51	2710	362	127	229	610	178
51	2190	508	13	76	610	44
76	5250	508	102	241	736	171

Table A-4. STAGNATION POINT HEAT TRANSFER RATES FOR PLUME IMPINGEMENT ON AN UNCONFINED CEILING

D (mm)	H (mm)	$\frac{H_f}{H}$	$\dot{Q}$ (W)	$\dot{q}''$ (w/m^2)	$\frac{\dot{q}''H^2}{\dot{Q}}$	Ra	$Ra^{1/6}\left(\frac{\dot{q}''H^2}{\dot{Q}}\right)$
Methanol							
10	61	0.21	59	20000	1.27	1.73×10^{7}	44.00
14	58	0.52	124	26600	0.73	3.36×10^{9}	28.25
18	127	0.42	165	5380	0.53	2.11×10^{10}	27.65
18	381	0.17	126	365	0.42	1.45×10^{11}	30.51
25	58	2.40	165	40000	0.90	4.48×10^{9}	36.50
25	381	0.37	250	653	0.39	2.89×10^{11}	31.47
35	616	0.25	301	549	0.58	1.08×10^{12}	59.05
76	775	0.33	1180	704	0.36	5.62×10^{12}	47.73
76	940	0.27	1190	460	0.34	8.33×10^{12}	48.40
Ethanol							
10	61	0.21	54	16370	1.11	1.61×10^{9}	38.00
14	58	0.52	108	31180	0.98	3.20×10^{9}	37.62
18	127	0.44	177	6270	0.57	2.20×10^{10}	30.30
25	58	2.50	272	47200	0.59	7.38×10^{9}	26.03
51	629	0.36	707	542	0.30	2.20×10^{12}	34.55
76	775	0.46	1603	1230	0.46	7.65×10^{12}	64.57
76	940	0.38	1543	580	0.33	1.08×10^{13}	49.06
1-Propanol							
18	381	0.30	196	611	0.45	2.26×10^{11}	35.28
25	381	0.43	355	919	0.38	4.10×10^{11}	32.58
51	629	0.40	786	662	0.33	2.47×10^{12}	38.72
76	775	0.52	1850	934	0.30	8.83×10^{12}	43.13
76	940	0.43	1814	700	0.34	1.27×10^{13}	52.00

Table A-4. STAGNATION POINT HEAT TRANSFER RATES FOR PLUME IMPINGEMENT ON AN UNCONFINED CEILING (continued)

D (mm)	H (mm)	$\frac{H_f}{H}$	$\dot{Q}$ (W)	$\dot{q}''$ (w/m^2)	$\frac{\dot{q}''H^2}{\dot{Q}}$	Ra	$Ra^{1/6}\left(\frac{\dot{q}''H^2}{\dot{Q}}\right)$
n-Pentane							
18	381	0.52	471	944	0.29	5.44×10^{11}	26.20
25	381	0.58	750	1790	0.35	8.66×10^{11}	33.78
35	616	0.66	968	1084	0.43	2.90×10^{12}	50.75
76	775	0.52	3459	1479	0.26	1.65×10^{13}	41.00
76	940	0.46	3080	982	0.28	2.16×10^{13}	46.89

Table A-5. EFFECT OF FLAME IMPINGEMENT ON STAGNATION POINT HEAT TRANSFER RATES ON AN UNCONFINED CEILING

D(mm)	H(mm)	$\frac{H_f}{H}$	$\dot{Q}$(W)	$\dot{q}''$(w/m^2)	$\frac{\dot{q}''H^2}{\dot{Q}}$	Ra	$Ra^{1/6}(\frac{\dot{q}''H^2}{\dot{Q}})$
Methanol							
18	381	0.17	126	365	0.42	1.45×10^{11}	30.51
25	381	0.37	250	653	0.39	2.89×10^{11}	31.47
35	616	0.24	301	549	0.58	1.08×10^{12}	59.05
76	127	2.40	1198	24710	0.33	1.54×10^{11}	24.37
76	254	1.20	1156	7660	0.43	5.93×10^{11}	39.10
Ethanol							
18	381	0.27	177	538	0.44	2.04×10^{11}	33.76
35	622	0.32	408	352	0.24	1.26×10^{12}	33.28
51	629	0.36	707	542	0.30	2.20×10^{12}	34.55
76	76	4.33	1523	24100	9.19×10^{-2}	7.03×10^{10}	5.90
76	127	2.60	1740	22570	0.21	2.23×10^{11}	16.35
76	254	1.30	1523	8680	0.37	7.82×10^{11}	35.32
1-Propanol							
18	381	0.30	196	611	0.45	2.26×10^{11}	35.28
25	381	0.43	355	919	0.38	4.10×10^{11}	32.58
51	629	0.40	786	662	0.33	2.47×10^{12}	38.72
51	127	2.00	863	17139	0.32	1.11×10^{11}	22.18
76	76	5.17	1726	23430	7.88×10^{-2}	7.97×10^{10}	5.17
76	127	3.10	1726	35840	0.24	2.21×10^{11}	18.74
76	254	1.65	1726	12910	0.48	8.86×10^{11}	47.60

Table A-5. EFFECT OF FLAME IMPINGEMENT ON STAGNATION POINT HEAT TRANSFER RATES ON AN UNCONFINED CEILING (continued)

D (mm)	H (mm)	$\frac{H_f}{H}$	$\dot{Q}$ (W)	$\dot{q}''$ (w/m^2)	$\frac{\dot{q}''H^2}{\dot{Q}}$	Ra	$Ra^{1/6}(\frac{\dot{q}''H^2}{\dot{Q}})$
n-Pentane							
18	381	0.50	471	944	0.29	5.44×10^{11}	26.20
25	381	0.58	750	1790	0.35	8.66×10^{11}	33.78
35	616	0.66	968	1084	0.42	2.90×10^{12}	50.75
51	629	0.53	1400	1722	0.49	4.40×10^{12}	62.21
51	127	2.80	1578	25400	0.26	2.02×10^{11}	19.85
76	76	6.67	3416	22380	0.038	1.58×10^{11}	2.80
76	127	4.00	3078	27170	0.12	4.32×10^{11}	10.50

Table A-6. CEILING HEAT FLUXES FOR PLUME IMPINGEMENT ON AN UNCONFINED CEILING.

H (mm)	$\frac{r}{H}$	D (mm)	$\dot{Q}$ (W)	$\dot{q}''$ (w/m^2)	$\frac{\dot{q}'' H^2}{\dot{Q}}$	Ra
Methanol						
220	0.23	35	357	2080	0.29	1.37×10^{11}
220	0.34	35	351	1390	0.19	1.35×10^{11}
220	0.91	35	351	221	3.10×10^{-2}	1.35×10^{11}
381	0.13	18	126	365	0.42	1.45×10^{11}
381	0.13	25	250	653	0.39	2.89×10^{11}
381	0.80	25	238	108	6.42×10^{-2}	2.75×10^{11}
616	0.08	35	357	549	0.58	1.08×10^{12}
616	0.13	35	366	353	0.38	1.10×10^{12}
616	0.33	35	366	153	0.16	1.10×10^{12}
58	0	14	124	26600	0.73	3.36×10^{9}
127	0	18	165	5380	0.53	2.11×10^{9}
775	0	76	1177	704	0.36	5.62×10^{12}
940	0	76	1186	460	0.34	8.33×10^{12}

Table A-6. CONTINUED

H(mm)	$\frac{r}{H}$	D(mm)	$\dot{Q}$(W)	$\dot{q}''$ (w/m^2)	$\frac{\dot{q}'' H^2}{\dot{Q}}$	Ra
Ethanol						
220	0.23	35	448	2290	0.25	1.72×10^{11}
220	0.34	35	432	1800	0.21	1.66×10^{11}
220	0.91	35	432	280	3.19×10^{-2}	1.66×10^{11}
381	0.13	18	177	538	0.44	2.04×10^{11}
381	0.47	18	174	203	0.17	2.00×10^{11}
381	0.80	18	174	71	5.94×10^{-2}	2.00×10^{11}
622	0.08	35	408	352	0.32	1.26×10^{12}
622	0.12	35	408	336	0.32	1.26×10^{12}
622	0.29	35	408	269	0.26	1.26×10^{12}
127	0	18	177	6270	0.57	2.26×10^{10}
775	0	76	1603	1230	0.46	7.65×10^{12}
940	0	76	1543	580	0.33	1.08×10^{13}

Table A-6. CONTINUED

H(mm)	$\frac{r}{H}$	D(mm)	$\dot{Q}$(W)	$\dot{q}''$ (w/m^2)	$\frac{\dot{q}'' H^2}{Q}$	Ra
1-propanol						
220	0.23	35	485	2320	0.24	1.87×10^{11}
220	0.34	35	494	2230	0.22	1.90×10^{11}
220	0.91	35	494	330	3.30×10^{-2}	1.90×10^{11}
381	0.13	18	196	611	0.45	2.26×10^{11}
381	0.47	18	175	210	0.17	2.02×10^{11}
381	0.80	18	175	82	6.77×10^{-2}	2.02×10^{11}
381	0.13	25	355	919	0.37	4.10×10^{11}
381	0.20	25	355	736	0.30	4.10×10^{11}
381	0.47	25	355	602	0.25	4.10×10^{11}
381	0.53	25	355	352	0.15	4.10×10^{11}
381	0.80	25	355	223	8.03×10^{-2}	4.10×10^{11}
622	0.08	35	389	392	0.39	1.20×10^{12}
622	0.12	35	389	336	0.33	1.20×10^{12}
622	0.29	35	389	251	0.25	1.20×10^{12}
775	0	76	1850	934	0.30	8.83×10^{12}
940	0	76	1814	700	0.34	1.27×10^{13}

Table A-6. CONTINUED

H(mm)	$\frac{r}{H}$	D(mm)	$\dot{Q}$(W)	$\dot{q}''$ (w/m^2)	$\frac{\dot{q}'' H^2}{\dot{Q}}$	Ra
n-pentane						
220	0.34	25	642	2540	0.20	2.50×10^{11}
220	0.91	25	642	400	3.03×10^{-2}	2.50×10^{11}
381	0.13	18	471	944	0.29	5.44×10^{11}
381	0.47	18	509	412	0.12	5.88×10^{11}
381	0.80	18	509	168	4.78×10^{-2}	5.88×10^{11}
381	0.13	25	750	1790	0.35	8.66×10^{11}
381	0.20	25	750	1230	0.24	8.66×10^{11}
381	0.47	25	755	937	0.18	8.72×10^{11}
381	0.53	25	750	774	0.15	8.66×10^{11}
381	0.80	25	755	416	8.03×10^{-2}	8.72×10^{11}
616	0.08	35	968	1084	0.42	2.90×10^{12}
616	0.33	35	928	360	0.15	2.80×10^{12}
775	0	76	3459	1479	0.26	1.65×10^{13}
940	0	76	3080	982	0.28	2.16×10^{13}

Table A-7. CEILING HEAT FLUXES FOR FLAME IMPINGEMENT ON AN UNCONFINED CEILING

H(mm)	$\frac{r}{H}$	D(mm)	$\dot{Q}$(W)	$\dot{q}''$ (w/m^2)	$\frac{\dot{q}'' H^2}{Q}$	Ra
Methanol						
220	0.23	51	641	3680	0.28	25.00×10^{11}
220	0.34	51	641	2190	0.17	25.00×10^{11}
220	0.80	51	641	766	6.00×10^{-2}	25.00×10^{11}
220	0.91	51	641	347	2.76×10^{-2}	25.00×10^{11}
220	1.37	51	641	352	2.76×10^{-2}	25.00×10^{11}
220	0.23	76	1176	5250	0.22	4.53×10^{11}
220	0.34	76	1132	3530	0.15	4.36×10^{11}
220	0.80	76	1117	1469	6.50×10^{-2}	4.30×10^{11}
220	0.91	76	1132	599	2.61×10^{-2}	4.36×10^{11}
220	1.37	76	1117	826	3.65×10^{-2}	4.30×10^{11}
127	0	76	1198	24710	0.33	1.54×10^{11}
127	1	76	1198	2940	3.96×10^{-2}	1.54×10^{11}
127	1	76	1198	5170	6.96×10^{-2}	1.54×10^{11}
127	2	76	1157	1410	1.96×10^{-2}	1.48×10^{11}
127	2	76	1157	1050	1.46×10^{-2}	1.48×10^{11}
254	0	76	1156	7660	0.43	5.93×10^{11}

Table A-7. CONTINUED

H(mm)	$\frac{r}{H}$	D(mm)	$\dot{Q}$(W)	$\dot{q}''$ (w/m^2)	$\frac{\dot{q}'' H^2}{Q}$	Ra
Ethanol						
127	0	76	1740	22570	0.21	2.23×10^{11}
127	1	76	1740	2800	2.60×10^{-2}	2.23×10^{11}
127	1	76	1740	6310	5.85×10^{-2}	2.23×10^{11}
127	2	76	1631	1091	1.08×10^{-2}	2.10×10^{11}
127	2	76	1631	1073	1.06×10^{-2}	2.10×10^{11}
254	0	76	1523	8680	0.37	7.82×10^{11}
254	0.5	76	1560	2970	0.12	8.00×10^{11}
254	1	76	1523	838	3.55×10^{-2}	7.82×10^{11}
254	1	76	1523	737	3.12×10^{-2}	7.82×10^{11}

Table A-7. CONTINUED

H(mm)	$\frac{r}{H}$	D(mm)	$\dot{Q}$(W)	$\dot{q}''$ (w/m^2)	$\frac{\dot{q}'' H^2}{Q}$	Ra
1-Propanol						
127	0	51	863	17139	0.32	1.11×10^{11}
127	1	51	863	1284	2.40×10^{-2}	1.11×10^{11}
127	1	51	863	3682	6.88×10^{-2}	1.11×10^{11}
127	2	51	801	556	1.12×10^{-2}	1.03×10^{11}
127	2	51	801	528	1.06×10^{-2}	1.03×10^{11}
127	0	76	1726	25840	0.24	2.21×10^{11}
127	1	76	1726	5590	5.22×10^{-2}	2.21×10^{11}
127	1	76	1726	3600	3.36×10^{-2}	2.21×10^{11}
127	2	76	1788	1510	1.36×10^{-2}	2.30×10^{11}
254	0	76	1726	12910	0.48	8.86×10^{11}
254	0.5	76	1808	3460	0.12	9.28×10^{11}
254	1	76	1726	810	3.03×10^{-2}	8.86×10^{11}

Table A-7. CONTINUED

H(mm)	$\frac{r}{H}$	D(mm)	$\dot{Q}$(W)	$\dot{q}''$ (w/m^2)	$\frac{\dot{q}'' H^2}{Q}$	Ra
n-Pentane						
220	0.23	51	1490	9420	0.31	5.74×10^{11}
220	0.34	51	1490	8780	0.29	5.74×10^{11}
220	0.80	51	1490	2256	0.08	5.74×10^{11}
220	0.91	51	1490	1310	0.04	5.74×10^{11}
220	1.37	51	1490	1249	0.04	5.74×10^{11}
220	0.23	76	3660	18680	0.25	1.41×10^{12}
220	0.34	76	3850	15400	0.20	1.48×10^{12}
220	0.80	76	3810	5330	0.07	1.47×10^{12}
220	0.91	76	3850	2360	0.03	1.48×10^{12}
220	1.37	76	3810	1870	0.02	1.47×10^{12}
127	0	51	1578	25400	0.26	2.02×10^{11}
127	1	51	1578	2386	2.44×10^{-2}	2.02×10^{11}
127	1	51	1578	8760	8.95×10^{-2}	2.02×10^{11}
127	0	35	1224	22930	0.30	1.57×10^{11}
127	1	35	1224	2720	3.58×10^{-2}	1.57×10^{11}
127	1	35	1224	2190	2.88×10^{-2}	1.57×10^{11}
127	2	35	1051	837	1.28×10^{-2}	1.35×10^{11}
127	2	35	1051	906	1.39×10^{-2}	1.35×10^{11}

Continued, next page

H (mm)	$\frac{r}{H}$	D (mm)	$\dot{Q}$ (W)	$\dot{q}''$ (w/m^2)	$\frac{\dot{q}'' H^2}{Q}$	Ra
127	2	76	3328	2670	1.29×10^{-2}	4.27×10^{11}
254	0	76	3415	15760	0.30	1.73×10^{12}
254	1	76	3415	1910	3.60×10^{-2}	1.73×10^{12}
254	0.5	76	3564	6300	0.11	1.83×10^{12}
254	0.5	76	3564	5240	9.48×10^{-2}	1.83×10^{12}

Table A-8. CEILING HEAT FLUXES FOR PLUME IMPINGEMENT ON A CONFINED CEILING (L = 152 mm)

H(mm)	$\frac{r}{H}$	D(mm)	$\dot{Q}$(W)	$\dot{q}''$ (w/m^2)	$\frac{\dot{q}'' H^2}{Q}$	Ra
Methanol						
457	0	76	1094	1898	0.36	1.82×10^{12}
457	0.28	76	1094	1124	0.21	1.82×10^{12}
457	0.28	76	1094	1139	0.22	1.82×10^{12}
457	0.56	76	1094	684	0.13	1.82×10^{12}
457	0	51	587	1163	0.41	9.76×10^{11}
457	0.28	51	587	584	0.21	9.76×10^{11}
457	0.28	51	587	668	0.24	9.76×10^{11}
457	0.56	51	615	416	0.14	1.02×10^{12}

Table A-8. CONTINUED

H(mm)	$\frac{r}{H}$	D(mm)	$\dot{Q}$(W)	$\dot{q}''$ (w/m^2)	$\frac{\dot{q}'' H^2}{Q}$	Ra
Ethanol						
457	0	76	1523	2589	0.36	2.53×10^{12}
457	0.28	76	1523	1532	0.21	2.53×10^{12}
457	0.28	76	1523	1614	0.22	2.53×10^{12}
457	0.56	76	1540	616	0.08	2.56×10^{12}
457	0	51	824	1520	0.39	1.37×10^{12}
457	0.28	51	824	845	0.21	1.37×10^{12}
457	0.28	51	824	850	0.22	1.37×10^{12}
457	0.56	51	780	384	0.10	1.30×10^{12}

Table A-8. CONTINUED

H(mm)	$\frac{r}{H}$	D(mm)	$\dot{Q}$(W)	$\dot{q}''$ (w/m^2)	$\frac{\dot{q}'' H^2}{Q}$	Ra
1-Propanol						
457	0	76	1757	3330	0.40	2.92×10^{12}
457	0.28	76	1757	1753	0.21	2.92×10^{12}
457	0.28	76	1757	1765	0.21	2.92×10^{12}
457	0.56	76	1763	782	0.09	2.93×10^{12}
457	0	51	934	1984	0.44	1.55×10^{12}
457	0.28	51	934	1200	0.27	1.55×10^{12}
457	0.28	51	934	1235	0.28	1.55×10^{12}
457	0.56	51	934	520	0.12	1.55×10^{12}

Table A-9. CEILING HEAT FLUXES FOR PLUME IMPINGEMENT ON A CONFINED CEILING (L = 305 mm)

H(mm)	$\frac{r}{H}$	D(mm)	$\dot{Q}$(W)	$\dot{q}''$ (w/m^2)	$\frac{\dot{q}'' H^2}{Q}$	Ra
Methanol						
457	0	51	647	1823	0.59	1.08×10^{12}
457	0.28	51	647	1134	0.37	1.08×10^{12}
457	0.28	51	647	1129	0.37	1.08×10^{12}
457	0.56	51	702	518	0.15	1.17×10^{12}
457	0	51	746	1910	0.53	1.24×10^{12}
457	0.28	51	746	1500	0.42	1.24×10^{12}
457	0.28	51	746	1480	0.41	1.24×10^{12}
457	0.56	51	614	577	0.22	1.02×10^{12}
Ethanol						
457	0	51	925	2946	0.67	1.54×10^{12}
457	0.28	51	925	1779	0.40	1.54×10^{12}
457	0.28	51	925	1730	0.39	1.54×10^{12}
457	0.56	51	982	700	0.15	1.63×10^{12}
457	0	51	910	2710	0.62	1.51×10^{12}
457	0.28	51	910	1700	0.39	1.51×10^{12}
457	0.56	51	968	837	0.18	1.61×10^{12}

Table A-9. CONTINUED

H(mm)	$\frac{r}{H}$	D(mm)	$\dot{Q}$(W)	$\dot{q}''$ (w/m^2)	$\frac{\dot{q}'' H^2}{Q}$	Ra
1-Propanol						
457	0	51	1048	3020	0.60	1.74×10^{12}
457	0.28	51	1048	1916	0.38	1.74×10^{12}
457	0.28	51	1048	1658	0.33	1.74×10^{12}
457	0.56	51	999	751	0.16	1.66×10^{12}
457	0	51	999	2126	0.45	1.66×10^{12}

Table A-10. CEILING PLUME TEMPERATURES (NO CURTAIN WALL)

H = 695 mm H_f = 89 mm T_∞ = 26.4 C

H_p = 356 mm $\dot{Q}$ = 243 W Methanol

r(mm)	$T - T_\infty$(C)	r(mm)	$T - T_\infty$(C)
0	61.9	41.0	21.4
3.0	61.7	44.5	18.6
6.0	57.9	47.5	17.6
9.5	57.6	51.0	12.3
16.0	55.0	54.0	9.6
19.0	50.3	57.0	9.2
22.0	47.1	60.0	7.0
25.5	41.9	63.5	6.2
28.5	39.2	66.5	5.8
32.0	38.0	70.0	5.6
35.0	32.9	76.0	2.1
38.0	28.1		

Table A-10. CONTINUED

H = 695 mm H_f = 89 mm T_∞ = 27.64 C

H_p = 483 mm $\dot{Q}$ = 245 W Methanol

r(mm)	$T - T_\infty$(C)	r(mm)	$T - T_\infty$(C)
0	43.5	41.0	26.2
3.0	42.0	44.5	24.4
6.5	38.1	47.5	24.0
9.5	37.7	54.0	19.3
12.5	37.2	60.0	18.2
16.0	36.1	66.5	14.7
19.0	34.1	70.0	13.2
22.0	33.9	76.0	9.6
25.5	31.7	82.5	7.0
28.5	29.9	89.0	5.0
32.0	28.6	95.0	3.9
35.0	28.3	101.5	2.5
38.0	26.8	108.0	1.1

Table A-10. CONTINUED

H = 695 mm H_f = 89 mm T_∞ = 27.78 C

H_p = 584 mm $\dot{Q}$ = 246 W Methanol

r(mm)	$T - T_\infty$(C)	r(mm)	$T - T_\infty$(C)
0	28.2	38.0	23.7
3.0	27.5	44.5	21.6
6.5	27.7	51.0	17.9
9.5	28.3	57.5	16.7
12.5	27.7	63.5	14.5
16.0	28.0	70.0	13.8
19.0	27.7	76.0	11.0
22.0	27.0	82.5	8.5
25.5	25.9	89.0	6.8
28.5	26.3	95.0	5.6
32.0	24.4	101.5	2.9
35.0	24.2	108.0	1.8

Table A-11. CEILING JET TEMPERATURES (NO CURTAIN WALL)

H = 695 mm H_f = 89 mm T_∞ = 30.5 C

r = 0 mm $\dot{Q}$ = 257 W Methanol

y (mm)	$T-T_\infty$ (C)	y (mm)	$T-T_\infty$ (C)
2.5	25.9	40.5	25.4
5.0	25.2	43.0	26.2
7.5	25.6	46.0	25.8
10.0	25.8	48.0	26.8
12.5	25.1	51.0	25.9
15.0	26.0	53.0	27.1
18.0	25.8	56.0	26.8
20.0	24.4	58.5	27.2
23.0	25.0	61.0	26.5
25.5	25.2	66.0	26.6
28.0	25.3	71.0	27.5
30.5	24.3	76.0	27.7
33.0	24.4	102.0	30.3
35.5	25.9	127.0	30.2
38.0	25.9		

Table A-11. CEILING JET TEMPERATURES (NO CURTAIN WALL) (continued)

$H = 695$ mm $\quad H_f = 89$ mm $\quad T_\infty = 30.5$ C

$r = 76.2$ mm $\quad \dot{Q} = 257$ W $\quad$ Methanol

y (mm)	$T-T_\infty$ (C)	y (mm)	$T-T_\infty$ (C)
2.5	22.5	40.5	12.1
5.0	23.1	43.0	12.1
7.5	22.6	45.5	12.0
10.0	22.4	48.0	10.8
12.5	20.5	51.0	10.3
15.0	19.5	56.0	10.1
18.0	18.7	61.0	9.1
20.0	18.2	66.0	9.9
23.0	17.1	71.0	10.0
25.5	15.5	76.0	9.6
28.0	15.0	81.0	9.1
30.5	13.9	86.5	9.1
33.0	13.6	91.5	8.8
35.5	13.3	96.5	9.4
38.0	13.1	101.5	8.7
		127.0	9.1

Table A-11. CEILING JET TEMPERATURES (NO CURTAIN WALL) (continued)

$H = 695$ mm	$H_f = 89$ mm	$T_\infty = 29.4$ C
$r = 127$ mm	$\dot{Q} = 253$ W	Methanol

y (mm)	$T-T_\infty$ (C)	y (mm)	$T-T_\infty$ (C)
2.5	18.3	33.0	8.2
5.0	19.4	35.5	7.8
7.5	18.7	38.0	6.5
10.0	18.0	40.5	6.0
12.5	16.7	43.0	5.2
15.0	15.3	45.5	4.6
18.0	14.2	48.0	4.5
20.0	13.4	53.0	4.2
23.0	12.5	58.5	3.1
25.5	11.4	63.5	2.3
28.0	11.1	68.5	2.0
30.5	9.4		

Table A-11. CEILING JET TEMPERATURES (NO CURTAIN WALL) (continued)

$H = 695$ mm $\quad H_f = 89$ mm $\quad T_\infty = 30.8$ C

$r = 203$ mm $\quad \dot{Q} = 248$ W $\quad$ Methanol

y (mm)	$T-T_\infty$ (C)	y (mm)	$T-T_\infty$ (C)
2.5	12.3	30.5	7.2
5.0	14.3	33.0	6.0
7.5	14.2	35.5	6.1
10.0	13.2	38.0	5.0
12.5	12.9	40.5	4.5
15.0	12.6	43.0	3.5
18.0	11.4	45.5	3.0
20.5	10.7	48.0	2.7
23.0	9.8	53.0	1.8
25.5	8.7	58.5	1.6
28.0	8.0		

Table A-11. CEILING JET TEMPERATURES (NO CURTAIN WALL) (continued)

H = 695 mm H_f = 89 mm T_∞ = 31.1 C

r = 254 mm $\dot{Q}$ = 255 W Methanol

y (mm)	$T-T_\infty$ (C)	y (mm)	$T-T_\infty$ (C)
2.5	11.2	33.0	7.6
5.0	12.2	35.5	7.1
7.5	12.2	38.0	6.2
10.0	12.0	40.5	5.2
12.5	11.5	43.0	5.1
15.0	11.0	45.5	4.4
18.0	10.7	48.0	3.3
20.0	10.5	51.0	3.1
23.0	9.7	56.0	2.2
25.5	9.5	61.0	1.4
28.0	8.8	66.0	1.3
30.5	8.5	71.0	1.1

Table A-12. CEILING PLUME TEMPERATURES
(Curtain Wall L=241 mm, D_c=610 mm)

H = 695 mm H_f = 89 mm T_∞ = 25.56 C

H_p = 356 mm $\dot{Q}$ = 245 W Methanol

r(mm)	$T - T_\infty$(C)	r(mm)	$T - T_\infty$(C)
0	65.7	41.3	22.2
3.0	64.4	44.5	21.4
6.5	65.0	47.5	17.3
9.5	62.7	51.0	15.2
12.5	62.1	54.0	11.8
16.0	60.0	57.0	9.7
19.0	58.3	60.0	6.1
22.0	54.0	63.5	5.2
25.5	48.9	66.5	3.3
28.5	46.0	73.0	3.0
32.0	41.6	79.5	1.1
35.0	36.4	85.5	0.7
38.0	28.1	92.0	0.5

Table A-12. CONTINUED

H = 695 mm H_f = 89 mm T_∞ = 23.3 C

H_p = 483 mm $\dot{Q}$ = 245 W Methanol

r(mm)	$T - T_\infty$(C)	r(mm)	$T - T_\infty$(C)
0	37.2	41.0	25.4
3.0	35.6	44.5	24.3
6.5	36.6	47.5	22.3
9.5	36.1	51.0	21.5
12.5	36.6	54.0	19.3
16.0	35.0	57.0	19.0
19.0	33.3	60.0	18.2
22.0	31.8	66.5	16.8
25.5	31.4	73.0	15.7
28.5	30.1	79.5	15.4
32.0	29.2	85.5	14.9
35.0	27.6	92.0	14.4
38.0	27.7	98.5	14.4

Table A-12. CONTINUED

H = 695 mm H_f = 89 mm T_∞ = 25.0 C

H_p = 610 mm $\dot{Q}$ = 242 W Methanol

r(mm)	$T - T_\infty$(C)	r(mm)	$T - T_\infty$(C)
0	32.0	38.0	26.3
3.0	32.0	41.0	25.3
6.5	32.0	44.5	24.8
9.5	31.5	51.0	24.1
12.5	31.2	57.0	22.7
16.0	30.5	63.5	21.9
19.0	29.3	70.0	21.2
22.0	28.3	76.0	21.0
25.5	28.2	82.5	19.8
28.5	27.3	89.0	19.7
31.5	27.2	95.0	19.5
35.0	26.9	101.5	19.6

Table A-13. CEILING JET TEMPERATURES
(CURTAIN WALL, L = 241 mm, D_c = 610 mm)

H = 695 mm H_f = 89 mm T_∞ = 25.7 C

r = 0 mm $\dot{Q}$ = 242 W Methanol

y (mm)	$T-T_\infty$ (C)	y (mm)	$T-T_\infty$ (C)
4.0	29.5	29.5	29.2
6.5	29.3	32.0	29.6
9.0	29.5	34.5	29.9
11.5	29.3	37.0	30.2
14.0	29.4	39.5	30.0
17.0	29.5	42.0	29.8
19.0	29.2	45.0	30.3
22.0	29.3	47.0	29.9
24.5	29.3	50.0	31.2
27.0	29.4	52.0	31.0
55.0	30.0	106.0	33.5
57.0	30.6	116.0	33.3
60.0	31.0	126.0	34.6
62.5	30.5	136.0	35.5
65.0	31.4	149.0	36.0
70.0	31.4	161.5	37.3
75.0	31.2	174.0	36.5
80.0	30.8	199.5	39.7
85.0	31.7	225.0	44.1
90.5	32.7	250.5	45.3
95.5	32.5	276.0	48.6
100.5	32.6	301.0	53.4

Table A-13. CEILING JET TEMPERATURES
(Curtain Wall, L = 241 mm, D_c = 610 mm)
(continued)

H = 695 mm H_f = 89 mm T_∞ = 28.1 C

r = 76 mm $\dot{Q}$ = 254 W Methanol

y (mm)	$T-T_\infty$ (C)	y (mm)	$T-T_\infty$ (C)
2.5	29.3	86.5	21.1
5.0	29.6	91.5	21.3
7.5	29.7	96.5	21.3
10.0	28.9	101.5	21.3
12.5	28.8	114.0	21.0
15.0	28.3	127.0	20.7
18.0	27.7	139.5	19.8
20.0	27.3	152.5	20.1
23.0	26.8	165.0	19.4
25.5	26.3	178.0	18.2
28.0	25.9	190.5	17.4
30.5	25.1	203.0	17.5
33.0	24.4	216.0	16.0
35.5	24.6	228.5	15.1
38.0	24.2	231.5	14.2
40.5	24.2	233.5	12.5
43.0	23.5	236.0	12.9
45.5	23.3	241.0	11.6
48.5	23.2	243.5	10.2
51.0	22.8	246.5	10.0
56.0	22.6	249.0	9.2
61.0	22.7	251.5	7.0
66.0	22.7	254.0	6.1
71.0	22.6	256.5	7.1
76.0	22.3	266.5	4.6
81.5	22.1	279.5	5.5
		292.0	3.8
		304.5	5.7
		312.5	3.6

Table A-13. CEILING JET TEMPERATURES
(CURTAIN WALL, L = 241 mm, D_c = 610 mm)
(continued)

H = 695 mm H_f = 89 mm T_∞ = 25.28 C

r = 127 mm $\dot{Q}$ = 247 W Methanol

y (mm)	$T-T_\infty$ (C)	y (mm)	$T-T_\infty$ (C)
3.0	23.4	102.0	17.6
5.5	23.8	115.0	17.4
8.0	24.0	127.5	17.4
10.5	23.4	140.0	17.4
13.0	23.4	153.0	17.7
15.5	22.6	165.5	17.1
18.5	22.7	178.0	16.8
21.0	22.4	191.0	16.2
23.5	21.7	203.5	15.0
26.0	20.9	216.5	13.5
28.5	20.7	229.0	10.4
31.0	20.5	231.5	9.7
36.0	19.5	236.5	7.7
41.0	19.1	242.0	6.9
46.0	18.8	247.0	4.1
51.5	18.3	252.0	3.2
56.5	18.5	244.0	4.9
61.5	18.3	257.0	2.3
66.5	17.8	262.0	3.6
71.5	17.9	267.0	2.2
76.5	18.0	280.0	1.9
89.5	17.9	293.0	1.9

Table A-13. CEILING JET TEMPERATURES
(CURTAIN WALL, L = 241 mm, D_c = 610 mm)
(continued)

H = 695 mm H_f = 89 mm T_∞ = 25.83 C

r = 203 mm $\dot{Q}$ = 246 W Methanol

y (mm)	$T-T_\infty$ (C)	y (mm)	$T-T_\infty$ (C)
3.0	18.5	176.0	18.6
5.5	20.2	188.5	18.8
8.0	20.7	201.0	18.5
10.5	21.2	214.0	17.7
13.0	21.0	226.5	16.5
15.5	20.9	229.0	16.1
18,0	20.9	231.5	15.7
21.0	21.1	234.0	16.9
23.5	20.6	236.5	14.1
28.5	19.8	239.0	14.0
33.5	19.5	242.0	12.6
38.5	18.8	244.0	11.3
43.5	18.6	247.0	10.6
49.0	18.0	249.5	9.8
54.0	18.1	252.0	8.0
59.0	18.1	254.5	6.9
64.0	17.7	257.0	8.0
69.0	17.8	259.5	6.4
74.0	17.6	262.0	4.6
87.0	17.7	264.5	3.2
99.5	17.7	267.0	2.2
125.0	18.0	272.0	2.5
137.5	17.6	275.0	1.4
150.5	18.3	287.5	1.3
163.0	18.4	300.0	1.3

Table A-13. CEILING JET TEMPERATURES
(CURTAIN WALL, L = 241 mm, D_c = 610 mm)
(continued)

H = 695 mm H_f = 89 mm T_∞ = 26.25 C

r = 254 mm $\dot{Q}$ = 244 W Methanol

y (mm)	$T-T_\infty$ (C)	y (mm)	$T-T_\infty$ (C)
3.0	13.3	168.0	18.7
5.5	16.2	181.0	19.1
8.0	18.3	193.5	19.0
10.5	19.2	206.0	19.1
13.0	19.8	219.0	18.7
15.5	19.9	229.0	18.5
18.0	20.3	231.5	18.4
21.0	20.4	234.0	18.1
23.5	20.3	236.5	18.4
26.0	20.5	239.0	18.3
28.5	20.5	242.0	18.3
31.0	20.9	244.0	18.0
33.5	20.8	247.0	17.8
36.0	20.5	249.5	17.3
38.5	20.6	252.0	16.5
43.5	20.6	254.5	16.3
48.8	20.2	257.0	14.7
54.0	20.1	259.5	14.9
59.0	19.9	262.0	13.5
64.0	19.5	264.5	13.0
69.0	19.4	267.0	10.6
74.0	18.5	269.5	9.4
79.0	18.9	272.0	7.4
92.0	19.0	275.0	4.9
104.5	18.7	277.5	5.0
117.0	18.5	280.0	2.5
130.0	19.4	282.5	3.1
142.5	19.2	287.5	1.7
155.5	18.8	292.5	1.6
		305.0	1.7

NBS-114A (REV. 9-78)

U.S. DEPT. OF COMM. BIBLIOGRAPHIC DATA SHEET	1. PUBLICATION OR REPORT NO. NBS-GCR-79-188	[redacted]

4. TITLE AND SUBTITLE

An Investigation of Fire Impingement on a Horizontal Ceiling

5. Publication Date

October 1978

7. AUTHOR(S)

H.Z. You and G.M. Faeth

8. Performing Organ. Report No.

9. PERFORMING ORGANIZATION NAME AND ADDRESS

Mechanical Engineering Department
Pennsylvania State University
University Park, Pennsylvania

11. Contract/Grant No.

Grant No. 7-9020

12. SPONSORING ORGANIZATION NAME AND COMPLETE ADDRESS *(Street, City, State, ZIP)*

National Bureau of Standards
Department of Commerce
Washington, DC 20234

13. Type of Report & Period Covered

15. SUPPLEMENTARY NOTES

☐ Document describes a computer program; SF-185, FIPS Software Summary, is attached.

16. ABSTRACT *(A 200-word or less factual summary of most significant information. If document includes a significant bibliography or literature survey, mention it here.)*

This report discusses research completed under NBS Grant No. 7-9020, during the period September 1, 1977 to August 31, 1978. The investigation considers the processes which occur when a turbulent fire impinges upon a horizontal ceiling. Measurements were conducted to determine free flame heights, impinging flame lengths along the ceiling, ceiling heat fluxes and mean temperature distributions in the flow. Both unconfined and confined ceilings were considered. Theoretical analysis was completed in order to suggest simple methods for correlating the data.

The fire source was simulated by burning wicks soaked with liquid fuel (methanol, ethanol, 1-propanol and n-pentane). The range of test variables involved ceiling diameters of 610-660 mm, ceiling heights of 58-940 mm, wick diameters of 10-107 mm and curtain wall heights (for confined ceilings) as large as the ceiling height.

17. KEY WORDS *(six to twelve entries; alphabetical order; capitalize only the first letter of the first key word unless a proper name; separated by semicolons)*

Ceilings; experiments; flame size; temperature distribution; turbulent burning

18. AVAILABILITY ☒ Unlimited

☐ For Official Distribution. Do Not Release to NTIS

☐ Order From Sup. of Doc., U.S. Government Printing Office, Washington, DC 20402, SD Stock No. SN003-003-

☒ Order From National Technical Information Service (NTIS), Springfield, VA. 22161

19. SECURITY CLASS (THIS REPORT) UNCLASSIFIED

20. SECURITY CLASS (THIS PAGE) UNCLASSIFIED

21. NO. OF PRINTED PAGES 112

22. Price $6.50

USCOMM-DC

INSTRUCTIONS

FORM NBS-114A: BIBLIOGRAPHIC DATA SHEET. This Bibliographic Data Sheet is an NBS adaptation of the form prescribed by COSATI guidelines (Appendix F, NBS Manual for Scientific and Technical Communications).

Item 1 - Complete if information is available; otherwise Publication Office will complete later. If non-NBS publication, state "see item 15". (Enter other agency sponsor's report number if requested to do so, and enter NBSIR number under item 8).

Items 2, 3, 6, 10, 14 - Ignore, these are reserved for possible future use.

Items 4, 7 - Complete as shown on manuscript. When NBS-114A is resubmitted along with NBS-266, following publication of non-NBS media papers, these items must agree with published paper.

Items 5, 21, 22 - Leave blank, Publication Office will complete.

Item 8 - Leave blank unless other agency sponsor's number appears as Item 1; then enter NBSIR number here.

Item 9 - If not NBS, blank out and enter Grantee/Contractor name and address, or both if performed jointly.

Item 11 - Complete when applicable.

Item 12 - Enter NBS name and address, other agency sponsor's name and address, or both if joint sponsorship. State "same as item 9" when appropriate.

Item 13 - Enter "Interim", "Final", or period covered.

Item 15 - Enter other relevant information, i.e., related or superseded documents. Also used by Publication Office for Library of Congress catalog number, and entry of non-NBS media citation upon receipt of Form NBS-266 from author.

Item 16, 17 - Complete with special care. Guidance given in NBS Manual. Abstract must agree with the one in the published paper.

Item 18 - Indicate "Unlimited" - for open-literature documents cleared under NBS editorial procedures, or "For official distribution. Do not release to NTIS" - for limited, restricted, or need-to-know material. (See 5.1.4.2.1 of Brady memo dated January 16, 1973 "Reports to Sponsors.") Publication Office will mark appropriate "order" box and complete Stock No. when known.